Demonstration and technoeconomic analysis of dodecanol production from acetate using metabolically engineered *Escherichia coli*

Paul M. Perkovich[1], Yoel R. Cortés-Peña[1], Justin J. Baerwald[1], Thomas H. Graupmann[1], Theodore A. Chavkin[1], Shivangi Mishra[1], William T. Cordell[1], Victor M. Zavala[1], Brian F. Pfleger[1]

1. Department of Chemical and Biological Engineering, University of Wisconsin–Madison, Madison, WI 53706, USA

*Corresponding author (Correspondence should be addressed to: Brian F. Pfleger at E-mail: brian.pfleger@wisc.edu)

Abstract:

In a circular bioeconomy, the one-way conversion of petroleum to chemicals and CO_2 is replaced with processes that reduce CO_2 to energy carriers and useful materials that are returned to CO_2 upon combustion. A circular bioeconomy that relies on photosynthesis to generate sugars as the chief energy carrier and precursor to chemical building blocks has yet to overcome many recalcitrant aspects of plant-based photosynthesis, namely, high feedstock costs, arable land scarcity, food competition, and fertilizer overuse. Acetate is a potential sustainable energy carrier because it can be produced from CO_2 either electrocatalytically or by acetogens via the Wood-Ljungdahl pathway. In this work, we conducted a metabolic engineering study of *Escherichia coli's* ability to convert acetate into dodecanol as a model oleochemical product. We performed techno-economic and life cycle analyses to determine break-even points with alternative fossil fuel-based strategies and identified critical process performance parameters for supporting an industrial acetate-based bioprocess. These analyses showed that oleochemical yield is the primary driver of minimum oleochemical selling price and carbon intensity. Therefore, to increase yield on acetate, we deleted the *aceBAK* operon, which facilitates funneling of acetate into biomass instead of product. We performed additional strain engineering to increase flux towards dodecanol and increase acetate uptake. Finally, we demonstrated increased yield in controlled bioreactors, improving from 13% of the maximum theoretical yield to 37%. Rigorous uncertainty analyses assuming a range of market conditions and future technological performances resulted in 88% and 37% of simulated scenarios having lower carbon intensities than fossil fuel-based routes and lower minimum selling prices than the market price.

Keywords:

Metabolic engineering, acetate, oleochemicals, dodecanol, techno-economic analysis, life cycle analysis

1.1 Introduction:

The importance of reducing fossil fuel use is well known and difficult to understate. While progress is being made to replace fossil fuels as sources of electrical energy, sustainable routes to direct (termed “drop-in”) chemical replacements are needed for the manufacture of material goods, such as polymers and solvents, and for use in high energy density fuel applications such as aviation and diesel engines (Galán-Martín et al., 2021; Rahman et al., 2024). In this arena, biomanufacturing offers advantages over fossil fuel routes: operation at relatively mild temperatures and pressures, and the potential to utilize renewable feedstocks (Song and Prather, 2024). However, first-generation biomanufacturing strategies that use glucose from sugarcane, beets, or corn as biomanufacturing feedstocks must compete with human and animal nutritional needs (Galán-Martín et al., 2021; Zuiderveen et al., 2023). Furthermore, starch crop agriculture requires large amounts of fertilizer, often leading to over-use and downstream eutrophication, and contributes to arable land scarcity thereby motivating deforestation and biodiversity loss (Galán-Martín et al., 2021; Zuiderveen et al., 2023).

While biomanufacturing of some specialty chemicals (e.g., 1,3-propanediol, amino acids, citric acid) (Chen and Nielsen, 2016; Hermann, 2003; Kurian, 2005; Nakamura and Whited, 2003; Sun et al., 2015, 2018) with high selling prices (relative to glucose) have found industrial success,Click or tap here to enter text. the high cost of starch-derived glucose, relative to the selling price of fuels and commodity chemicals (e.g., sustainable aviation fuels - SAF, monomers for plastics), leaves little margin for operating costs or profit (Louw et al., 2023; Maitah and

Smutka, 2019; Watson et al., 2024; Wu et al., 2018; C. Zhang et al.,2025). This reality motivates the search for alternative biomanufacturing feedstocks (Pfleger and Takors, 2023). Despite substantial research and investment over forty years, second generation processes that convert lignocellulosic biomass into fermentable sugar streams have failed to overcome many of the originally identified hurdles to producing, harvesting, and processing the recalcitrant biopolymers (Long et al., 2025; Sulis et al., 2025). Direct photosynthetic chemical production using photoautotrophs (e.g., algae, plants, and cyanobacteria) has also been explored, but again with limited industrial success (Gifuni et al., 2019; Miao et al., 2020; Wichmann et al., 2021). Given the diversity of microbial metabolism, perhaps the time has come to consider sustainable alternatives to photosynthesis-derived energy carriers as biomanufacturing feedstocks.

In a circular economy, any alternative energy carrier must begin with CO_2 fixation and reduction. The Wood-Ljungdahl pathway (WLP), which uses H_2 to fuse two C_1 gases and produce a C_2 compound (i.e., acetyl-CoA, ethanol, acetate, acetone), is the most energetically efficient natural carbon fixation pathway (Bar-Even et al., 2012; Gasparrini et al., 2025). It is used by acetogens to anaerobically produce acetate and other mixtures of C_2 compounds from synthesis gas streams (CO, CO_2, H_2), offering the advantage of using cheap industrial waste streams and green hydrogen from water electrolysis as feedstocks. Commercial production of ethanol and acetate from waste steel mill gases has been demonstrated (Herwig et al., 2020; Liew et al., 2016) and is being championed as a carbon-negative route to producing chemical building blocks. In biomanufacturing processes, acetate can be activated to the ubiquitous biological building block, acetyl-CoA, opening a route to the production of a wide array of chemicals, like fatty acids, terpenoids, and biopolymers, from waste gases (Kiefer et al., 2021). Coupling the WLP to heterotrophic upgrading leverages the strengths of both organisms: efficient CO_2

fixation by acetogens while avoiding the ATP-costly Calvin-Benson-Bassham cycle and more advanced genetic toolkits and higher energy availability from aerobic metabolism in industrial heterotrophsClick or tap here to enter text., resulting in a higher theoretical yield compared to either organism on their own for almost all configurations of substrates and products (Gasparrini et al., 2025; Stark et al., 2022). Acetogens are an incredibly diverse class of organisms that can utilize a variety of C1 streams, even with gas pressures spanning multiple orders of magnitude, opening up routes from a range of C1 emission sources and energy sources (e.g., H_2, direct electron transfer via electrodes), and they are able to produce a range of C2 or C4 compounds (e.g., acetate, ethanol, isopropanol) for further upgrading by heterotrophs (Laura and Jo, 2023; Liew et al., 2022; Poehlein et al., 2025; Schuchmann and Müller, 2014). The tradeoff is increased capital cost and bioprocess complexity in sequential fermentations (Stark et al., 2022). For example, the issue of dilute intermediate acetic acid feeds has been studied using a continuous fermentation and cell recycle loops with *Moorella thermoacetica* and *Yarrowia lypolytica* to produce high titers and yields of lipids (Hu et al., 2016). Integrating acetogen-gas fermentation with a secondary bioreactor that upgrades acetate to a hydrophobic product is analogous to traditional gas-to-liquids (GTL) technologies (Braide et al., 2024; Daza and Kuhn, 2016; Wood et al., 2012) and has been called BioGTL (Pfleger, 2016).

Common biomanufacturing hosts such as *Escherichia coli* have been engineered to convert acetate into valuable chemicals including isobutanol, glycolate, 2,3-butanediol, polyhydroxyalkanoates, and acetone/isopropanol, which could theoretically be paired with acetogens to produce these compounds from CO_2 (Chen et al., 2018; Kiefer et al., 2021; Kutscha et al., 2024; Li et al., 2019; Novak et al., 2020; Ricci et al., 2025; Song et al., 2018). Of particular interest are processes that fully integrate acetogens and *E. coli* to convert syngas-

104 derived acetate into isopropanol, 3-hydroxypropionic acid, or hydroxybutyric acid, moving
105 beyond theory to demonstrate end to end CO_2-derived valuable chemicals(Lai et al., 2021;
106 Lehtinen et al., 2018; Yang et al., 2020; W. Zhang et al., 2025). In addition to overexpressing
107 biosynthetic genes and deleting competing pathways, strategies to increase chemical production
108 from acetate by and large focus on increasing acetate uptake, tailoring reducing equivalents
109 produced via the TCA cycle to those needed in the specific biosynthetic pathways, and
110 optimizing bioprocess conditions (Kiefer et al., 2021; Kutscha et al., 2024; Lai et al., 2021;
111 Lehtinen et al., 2018; Yang et al., 2020). As feedstock costs typically represent upwards of 50%
112 of operating costs across starch, biomass, or C1+H_2 feedstocks, there is an emphasis on
113 increasing the yield of bioprocesses to improve their commercial viability (C. Zhang et al.,
114 2025). Here, we investigated the conversion of acetate to model 12-carbon oleochemicals,
115 dodecanoic acid and dodecanol, in metabolically engineered *E. coli* strains.
116 Medium chain oleochemicals, comprising 8 to 14-carbon acyl chains, are an attractive
117 biomanufacturing target because of their low abundance in natural sources and the technical
118 advantages they provide to fuels, surfactants, and cosmetics compared to more abundant long-
119 chain compounds(Su et al., 2024). There have been extensive efforts to overproduce medium
120 chain length oleochemicals in *E. coli* from more standard substrates (i.e., glucose, glycerol, or
121 laboratory media) (Mehrer et al., 2018; Shin et al., 2016; Su et al., 2024; Youngquist et al.,
122 2013b). These largely focus on engineering chain length-specific thioesterases or reversing the
123 natural oleochemical degradation process (i.e., reverse β-oxidation) and have often reached g/L
124 titers(Hernández Lozada et al., 2020; Jindra et al., 2023; Mains et al., 2022; Shin et al., 2016;
125 Youngquist et al., 2013a, 2013b). Fatty acid production from acetate has been demonstrated in *E.*
126 *coli* via overexpression of the native thioesterase, *tesA* (Xiao et al., 2013), but this method is not

specific for medium chain oleochemicals, because *tesA* primarily produces C14-C16 compounds (Choi and Lee, 2013).

In this work, we engineered *E. coli*'s metabolism to increase the titer and yield of dodecanol in cultures fed acetate. Our envisioned process integrated the acetate upgrading bioreactor with an acetogen-driven gas fermentation such that CO_2 created as a respiratory byproduct of oleochemical synthesis could be recycled to the acetogens. The combined process would convert CO_2 and H_2 into oleochemicals – a potentially CO_2 negative biomanufacturing process. Our study integrated metabolic engineering, bioprocess design, and computational process modeling with an emphasis on strain and bioprocess design that will translate across scales. Techno-economic analysis (TEA) and life cycle analysis (LCA) identified product yield as the greatest influence on key process indicators, such as minimum selling price (MSP) and carbon intensity (CI). Guided by these findings, we increased the oleochemical yield by modifying the TCA cycle of *E. coli* to reduce flux towards biomass, which competes with dodecanol production. We also increased flux through limiting reactions in the acetate activation and terminal fatty alcohol biosynthetic pathways. Finally, we performed a bioreactor cultivation to optimize acetate feeding strategies. Our engineered strain increased the yield of fatty alcohols from 13% to 37% of the maximum theoretical yield on acetate. Our final bioprocess achieved a simulated MSP of 5.61 USD kg^{-1} compared to a 5.00 USD kg^{-1} benchmark for fossil-fuel based processes and a CI well below fossil fuel-based processes, demonstrating the benefit of using sustainably sourced acetate to synthesize petrochemical replacements.

Methods:

2.1 List of strains and plasmids used in this study:

Strain	Genotype	Source
TY30	MG1655 Δ*araBAD*, *ΔfadE*::P_{Trc}_*bte*, Δ*fadAB*:: P_{Trc}_*bte*, Φ(P_{Trc}-*fadD*)	(Youngquist et al., 2013b)
JB36	MG1655 Δ*araBAD*, Δ*fadE*:: P_{Trc}_*bte*, Δ*fadAB*:: P_{Trc}_*bte*, Φ(P_{Trc} -*fadD*), Δ*ldhA*:: P_{Trc}_^{Ma}*acr*	This work
TAC58	MG1655 Δ*araBAD*, Δ*fadE*:: P_{Trc}_*bte*, Δ*fadAB*:: P_{Trc}_*bte*, Φ(P_{Trc} -*fadD*), Δ*ldhA*::P_{Trc}_^{Ma}*acr* , Δ*aceBAK*	This work
PP20	MG1655 Δ*araBAD*, Δ*fadE*:: P_{Trc}_*bte*, Δ*fadAB*:: P_{Trc}_*bte* , Φ(P_{Trc} -*fadD*), Δ*ldhA*:: P_{Trc}_^{Ma}*acr*, Δ*aceBAK*, Δ*fadIJ*:: P_{Trc}_^{Ma}*acr*	This work
SM018	MG1655 Δ*araBAD*, Δ*fadE*:: P_{Trc}_*bte*, Δ*fadAB*:: P_{Trc}_*bte* , Φ(P_{Trc} -*fadD*), Δ*ldhA*:: P_{Trc}_^{Ma}*acr*, Δ*aceBAK*, Δ*poxB*:: P_{Trc}_*bte*	This work
PP21	MG1655 Δ*araBAD*, Δ*fadE*:: P_{Trc}_*bte*, Δ*fadAB*:: P_{Trc}_*bte* , Φ(P_{Trc} -*fadD*), Δ*ldhA*:: P_{Trc}_^{Ma}*acr*, Δ*aceBAK*, Δ*poxB*:: P_{Trc}_*bte,* Δ*fadIJ*:: P_{Trc}_^{Ma}*acr*	This work
PP22	MG1655 Δ*araBAD*, Δ*fadE*:: P_{Trc}_*bte*, Δ*fadAB*:: P_{Trc}_*bte* , Φ(P_{Trc} -*fadD*), Δ*ldhA*:: P_{Trc}_^{Ma}*acr*, Δ*aceBAK,* Δ*fadIJ*:: P_{Trc}_^{Ma}*acr*, Δ*fadK*::P_{Tet}_^{Ec}*ackA-pta*	This work
PP23	MG1655 Δ*araBAD*, Δ*fadE*:: P_{Trc}_*bte*, Δ*fadAB*:: P_{Trc}_*bte* , Φ(P_{Trc} -*fadD*), Δ*ldhA*:: P_{Trc}_^{Ma}*acr*, Δ*aceBAK,* Δ*fadIJ*:: P_{Trc}_^{Ma}*acr*, Δ*fadK*::P_{Tet}_^{Ec}*acs*	This work
PP24	MG1655 Δ*araBAD*, Δ*fadE*:: P_{Trc}_*bte*, Δ*fadAB*:: P_{Trc}_*bte* , Φ(P_{Trc} -*fadD*), Δ*ldhA*:: P_{Trc}_^{Ma}*acr*, Δ*aceBAK,* Δ*fadIJ*:: P_{Trc}_^{Ma}*acr*, Δ*fadK*::P_{Tet}_^{Se}*acs*(L641P)	This work
Plasmid	Relevant properties	
pBTRK_maACR	P_{Trc}_^{ma}*acr,* BBR1 origin, KmR	(Youngquist et al., 2013b)

Table 1. List of strains and plasmids used in this study.

2.2 Reagents and chemicals:

Chemicals were purchased from either Sigma Aldrich (St. Louis, MO) or Thermo Fisher Scientific (Waltham, MA), with the exception of MOPS free acid purchased from Dot Scientific (Burton, MI). Oligonucleotides were purchased from Integrated DNA Technologies (Coralville, IA) or Thermo Fisher Scientific (Waltham, MA). Enzymes were purchased from New England Biolabs (Ipswich, MA). DNA purification kits were purchased from Qiagen (Venlo,

Netherlands). MOPS minimal media was made using the standard formula: 40 mM MOPS, 4 mM Tricine, 0.525 mM $MgCl_2$, 9.5 mM NH_4Cl, 1.32 mM K_2HPO_4, 0.276 mM K_2SO_4, 0.01 mM $FeSO_4$, 5 μM $CaCl_2$, 50 mM NaCl (Neidhardt et al., 1974). LB broth was made using granulated premix.

2.3 Bacterial strain construction:

Integration of expression cassettes into the *E. coli* genome were carried out using lambda red recombinase-mediated homologous recombination with Cas9 counterselection, as described previously (Mehrer et al., 2018). Briefly, for insertions, strains expressing plasmid-based λ-Red recombinase and ^{Sp}Cas9 (on pMP11) were co-transformed with a linear dsDNA repair template with 500 bp of homology upstream and downstream to the desired locus and a plasmid transcribing a gRNA template that targets the WT sequence on the chromosome. Cells were plated on LB agar with carbenicillin and kanamycin to select for pMP11 and the gRNA plasmid. Cas9 selected for strains without the WT locus, and the desired payload integration was verified via colony PCR. For deletions, the Km^R gene was amplified with 25 bp of homology upstream and downstream of the desired locus and transformed without a gRNA plasmid, and cells were plated on LB agar with carbenicillin and kanamycin to select for pMP11 and the Km^R marker integration. To delete the integrated selection marker, Km^R, ssDNA oligo repair templates with 30 nucleotides of homology upstream and downstream of the Km^R marker were co-transformed with a gRNA plasmid targeting the Km^R marker. Cells were plated on carbenicillin and chloramphenicol to select for pMP11 and the gRNA plasmid, and the desired edit was confirmed via colony PCR. After verification of the desired insertion or deletion, gRNA plasmids were cured by inducing a gRNA transcribed by pMP11 targeting the BR322 origin of the gRNA

plasmid. After curing of the gRNA plasmid, the temperature sensitive pMP11 plasmid was cured by culturing overnight at 42°C. Plasmid curing was verified by streaking on agar plates with the appropriate antibiotics.

2.3 Bacterial culture:

For 5 mL production experiments, bacterial pre-seed cultures were inoculated from separate colonies for biological replicates into 5 mL of LB and grown overnight at 30°C. LB cultures were passaged into 5 mL seed cultures of MOPS minimal media with 2 g/L glucose and 5 g/L acetate and grown overnight at 30°C. 5 mL production cultures of MOPS minimal media (2 g/L glucose 5 g/L acetate, unless otherwise specified) were inoculated from mid-late exponential phase seeds (OD = 0.6 - 1.0) to a starting OD of 0.05, induced to 1 mM IPTG upon inoculation and grown for 5 days at 30°C. A 10% dodecane overlay (i.e., 0.5 mL for 5 mL of aqueous phase) was used to sequester fatty acid and alcohol products. Cultures were grown at 30°C for 5 days.

1 L Infors-HT Multifors bioreactors were used for bioreactor cultivation. Bioreactor cultures consisted of the same pre-seed LB culture method for biological replicates. MOPS minimal media with 4 g/L glucose and 5 g/L acetate was used in bioreactors and bioreactor seeds unless otherwise specified. Seed cultures consisted of 200 mL MOPS minimal media and were inoculated using 1-2 mL of dense LB culture. Seed cultures were grown to mid-exponential phase (OD = 0.4 – 0.6) at 30°C (~24 h) at which point culture volumes sufficient to inoculate 500 mL to OD = 0.05 were centrifuged and resuspended in 10 mL of fresh MOPS minimal media. Resuspended seed culture was used to inoculate bioreactors of 500 mL MOPS minimal media and 10% (50 mL) dodecane overlay. Bioreactors were kept at 30°C and sparged with 0.4 L/min sterile air with off-gas condensers, maintained at a pH 7.2 with 25% NH_4OH and 1M HCl,

and stirred at speeds between 250-500 rpm controlled by dissolved oxygen (DO) at a 40% setpoint. pH probes were calibrated with a 2-point calibration at 4.0 and 7.0, and DO probes were calibrated with a 1-point calibration of 100% by equilibrating uninoculated media for 1 hour at 30°C at maximum stirring and aeration. Bioreactor cultures were induced once the DO fell below 60%, indicating sufficient cell densities. 6 mL samples of emulsified aqueous and organic phase were taken at 24-hour intervals with final samples taken 144 hours (6 days) after inoculation. Concentrated 250 g/L acetate (from Na^+acetate) in water was used for bolus additions.

2.4 Analyte quantification:

For 5 mL production cultures and 6 mL bioreactor samples, 500 uL of aqueous phase was taken out for OD measurement and carbon (glucose and acetate) quantification. HPLC samples were prepared by pelleting cells in the aqueous phase and then filtering the supernatant through non-sterile 0.2 μm filters. Samples were run on a Rezex ROA-Organic Acid H+ (8%) LC column (300 x 7.8 mm) from Phenomenex with a mobile phase of 5 mM H_2SO_4 and an isocratic method run at 0.6 mL min^{-1} and a column temperature of 60°C on a Shimadzu HPLC system. Peak areas measured by RID were used to quantify glucose and acetate standards in MOPS media to create a linear standard curve, and experimental sample RID peak areas were used to calculate the acetate and glucose concentration.

For 5 mL production cultures, the remaining aqueous and organic phase mixture was used for oleochemical quantification, i.e., 4.5 mL of aqueous phase and 0.5 mL of dodecane organic phase. To reduce variability in bioreactor samples, the remaining mixture was used to create samples with precisely 4 mL of aqueous phase and 0.4 mL of dodecane organic phase. Internal standards consisted of C_{13} free fatty acid and fatty alcohol in 100% ethanol made in 100x stocks and added to samples to create 200 mg L^{-1} final concentrations, calculated using the

aqueous phase volume (i.e., 40 μL of 20 g L^{-1} internal standard was added to 4 mL of aqueous phase and 0.4 mL dodecane). External standards were created by adding C_{12} and C_{14} fatty acids and fatty alcohols from 100x stocks in ethanol to uninoculated media and dodecane samples to create a standard curve from 15.625 mg L^{-1} to 1,000 mg L^{-1}, calculated based on aqueous phase volume. After internal standard additions, all samples and external standards were acidified by adding 100 μL of glacial acetic acid and vortexing for 10s. 1 mL of hexane was added, samples were vortexed at 1200 rpm for 4 minutes and then centrifuged for 10:00 min at 3,000 g to separate the phases. 900 μL of organic phase was pipetted into GC vials for quantification. Organic phase samples were quantified via GC-MS on an Agilent J&W DB-FATWAX Ultra Inert column (30 m x 0.25 mm, 0.25 μm) with a method as follows: 120.0°C for 2:00, 140.0°C for 3:00 (ramp rate 5:00), 250.0°C for 6:00 (ramp rate 20:00). A split ratio of 20.0 was used with helium carrier gas.

To calculate yields from acetate in 5 mL production cultures, the titers from an equivalent culture in media with the same amount of glucose but no acetate were subtracted from the titers of the glucose and acetate culture and then divided by the amount of acetate consumed. The same seed culture was used to inoculate both glucose-only and glucose plus acetate conditions, i.e., titers were subtracted within biological replicates, yield was calculated for each replicate and then averaged. For bioreactor cultures, in a similar way, titers from samples taken at the time point when glucose was first fully depleted (as determined by DO nadir and confirmed afterwards via HPLC measurements of carbon) were subtracted from later titers to determine the amount of product synthesized from acetate and divided by the amount of acetate consumed to calculate yields from acetate. Maximum theoretical yields were calculated using a standard constraint-based metabolic model, as reported previously (Lennen and Pfleger, 2012; Pfleger et

al., 2015). Statistical tests used were ANOVA with Tukey-Kramer post-hoc test to compare dodecanol titers, yields, and acetate consumption across conditions. Welch's test (for cases of unequal variance) was used as post-hoc test for bioreactor comparisons.

2.5 Process Modeling

A computational model for the conceptual CO_2/H_2 to oleochemical process was developed in BioSTEAM, an open-source platform in Python for the design, simulation, and evaluation (via TEA and LCA) of biorefineries (Cortés-Peña, 2020; Cortes-Peña et al., 2020). The model builds upon existing TEA/LCA studies on gas-fed oleochemical production systems (Cortés-Peña et al., 2022; Li et al., 2023a). The main elements of the process model include acetate production, seed train, and oleochemical production (Figure 1). Three alternative configurations were evaluated: an "acetate" configuration where acetate is converted to dodecanol and bioreactor seed, a "acetate/glucose-seed" configuration where acetate is consumed to produce dodecanol while the glucose is consumed to produce the seed, and a "glucose" configuration where glucose is directly converted to dodecanol and seed, without acetate production (Figure 1). Due to the large amount of seed biomass required for the oleochemical bioreactor (0.45 $g_{product} \cdot g_{DCW}^{-1}$ under baseline assumptions), the selection of seed train substrate (glucose or acetate) can lead to significant differences in the potential economic viability and environmental impact.

The CO_2/H_2-fed acetic acid bioreactor was modeled as a continuous air-lift bioreactor with cell mass recirculation. Blast furnace flue gas—a byproduct of refining iron ore for steel production which is rich in CO_2 and CO—is fed to the bioreactor together with green hydrogen. Additionally, the CO_2-rich vent from the aerated bioreactor for oleochemical production is fed

back to the acetate bioreactor. The aerated oleochemical bioreactor (producing dodecanol) was modeled as an agitated batch bioreactor. The oleochemical product is excreted extracellularly and is readily separated with hexane as a non-polar solvent. The solvent is then recovered by distillation resulting in a >99.9 % pure product. The wastewater along with spent cell mass is sent to a multistage anaerobic wastewater treatment process designed for treating wastewaters with high organic loading rates distinctive to biorefinery wastewaters (Li et al., 2023b). The concentrated sludge and biogas from anaerobic digestion (both products of wastewater treatment) are burned together with biomass to supply steam for the oleochemical separation process. Renewable solar electricity was assumed to power the biorefinery. A detailed flowsheet is available in the SI (Figure S1).

The design procedure of the bioreactors follows the methodology described in recent TEA/LCA studies, which account for the pressure gradient across the vessel due to the liquid head using the log-mean driving force for mass transfer (Benz, 2011; Cortés-Peña et al., 2024). Briefly, the volumetric mass transfer coefficient, k_La (lumped together with the specific interfacial area), of the bubble column bioreactor producing acetate was estimated using the Dewes & Schumpe (1997) correlation, which relies only on the superficial gas velocity, viscosity of the liquid, and the density of the gas, without the need for detailed design of the bioreactor (Dewes and Schumpe, 1997). Given the flow rate of flue gas and green hydrogen, the total volume of all bioreactors (each of maximally 3,785 m^3) was solved numerically such that the effluent met the user specified titer (60 $g \cdot L^{-1}$ at baseline assumptions). The flow rate of green H_2 was set to the stoichiometric amount required to consume all CO_2 and CO from the feed. While gas-fed bioreactor designs typically have a height-to-diameter ratio of 3 to 5, this heuristic is only valid for aerobic processes that vent to the atmosphere. For the acetate bioreactor, a high

height-to-diameter ratio allowed more time for H_2 consumption (thereby improving yield). Additionally, because the vent from the oleochemical bioreactor is sent back to the acetate bioreactor, a high height-to-diameter ratio for the oleochemical bioreactor leads to a high CO_2 concentration (and low O_2 concentration) of gas sent to the acetate bioreactor. Therefore, a high height-to-diameter ratio in the downstream oleochemical bioreactor also improves CO_2/H_2 consumption at the upstream acetate bioreactor. An optimum height-to-diameter ratio of 12 was specified for all bioreactors. The k_La of the agitated bioreactor producing dodecanol was estimated using the Van't Riet's non-viscous mass transfer correlation (Van'T Riet, 1979). The flow rate of the air provided by the compressor (to the oleochemical bioreactor) was solved numerically such that the O_2 uptake rate was equal to the transfer rate at a dissolved concentration of 50% saturation (Benz, 2011; Humbird et al., 2017). The power consumed by the agitator was 0.3 $kW \cdot m^{-3}$ (a heuristic value recommended for industrial homogeneous reactions) (Seider et al., 2016). Additional process modeling assumptions are listed in Table S1 (SI).

2.6 Life Cycle Assessment (LCA)

The system boundary extends from cradle to biorefinery-gate for the operational phase and does not include the construction phase of the biorefinery. All operational inventory data (i.e., the life cycle inventory) originated from the biorefinery model leveraged in this study. The life cycle impact assessment methodology used was the Intergovernmental Panel on Climate Change (IPCC) 2013 (Stocker et al., 2013), with a focus on GWP_{100} as the primary indicator (reported herein as carbon intensity; CI). Life cycle inventory data for each raw material and ancillary input were adapted from the GREET 2023 model (Wang et al., 2023). The GREET model neither credits for CO_2 intake for plant growth, nor penalizes for biogenic CO_2 emissions. For biofuels, this form of accounting balances out due to how all end-of-life carbon emissions

originate from atmospheric carbon uptake (i.e., carbon neutrality). However, fatty alcohols serve a variety of end-uses (e.g., cosmetics, lubricant, plasticizers, surfactants) and stored carbon may not necessarily be combusted back to the environment. For this reason, here we credit the carbon intake for plant growth, in agreement with past LCA studies on fatty alcohols and other oleochemicals from both petrochemical and biological sources (Liew et al., 2025, 2022; Schowanek et al., 2018; Shah et al., 2016).

While the selection of a cradle-to-gate system boundary allows for negative carbon intensities to be computed when waste streams such as flue gas are consumed, it does not imply that the product has negative emissions over its entire life cycle (i.e., a cradle-to-grave system boundary). For example, it is possible that all dodecanol product is consumed to produce detergents that are ultimately digested to CO_2 by wastewater treatment. In this extreme case, it is impossible for the process to be carbon negative over the entire life cycle because all abated emissions from flue gas is ultimately released to the atmosphere at end-of-life disposal. Alternatively, all dodecanol can be used as plastic additive that is ultimately landfilled resulting in long-term carbon storage. Regardless of system boundary, the calculated reduction in carbon emissions relative to other pathways (e.g., fossil fuel-derived, palm oil-derived) would be the same as end-of-life fates would be applied equally to all pathways. More importantly, our selection of LCA methodology is standard for oleochemical products and allows us to directly compare with LCAs for different pathways (Liew et al., 2025, 2022; Schowanek et al., 2018; Shah et al., 2016).

2.7 Techno-Economic Analysis (TEA)

Cost correlations of specialized all equipment (e.g., bioreactors, compressors, heat exchangers, pumps) originate from various public sources (Perry et al., 1997; Seider et al., 2016),

as detailed by Cortes-Peña et al (Cortes-Peña et al., 2020). Cost correlations for utility systems including the co-heat and power generation, cooling tower, chilled water generation were adapted from the cellulosic ethanol biorefinery model of the National Renewable Energy Laboratory (NREL) (Humbird et al., 2011). All parameters used in the discounted cash flow analysis follow the assumptions made in NREL's cellulosic ethanol report (Humbird et al., 2011), except for the baseline federal corporate tax, which was updated to 21%. The price of renewable solar electricity was assumed to be 60 $USD \cdot MWh^{-1}$, the average price of renewable energy certificates in Maryland in 2023 (Barbose, 2024). The price of green hydrogen was assumed to vary uniformly between 2 to 6 $USD \cdot kg^{-1}$; the lower bound represents the optimistic forecast for H_2 from wind and solar electrolysis in 2030 (Castelvecchi, 2022), and the upper bound represents the potential H_2 price assuming existing technology, as estimated by the U.S. Department of Energy (Vickers et al., 2020). Material prices of other feeds come from various sources, including textbooks and literature (Humbird et al., 2011; "Materials Library | CatCost," n.d.; "Sugar - Price - Chart - Historical Data - News," n.d.; Thompson and Tyner, 2011). The minimum selling price (MSP) was the primary indicator used to compare the economic outcome of simulated scenarios. The Alibaba website (www.alibaba.com) was used to estimate market prices for high-volume orders for dodecanol. The following search criteria was used: search term: "Dodecanol"; filters applied on website: "trade assurance"; each listing considered must have a unique vendor; and only prices specified for orders ≥100 kg were considered. The preliminary survey of current selling prices for dodecanol shows a market price range of 2.09–8 $USD \cdot ton^{-1}$. For comparison purposes, we assume the MSP of dodecanol must be under 5.00 $USD \cdot ton^{-1}$ to be market competitive. A breakdown of the estimated revenue and capital and operating expenditures can be found in Tables S3–S5 (SI).

2.8 Accessing biorefinery models and detailed results

All biorefinery source code and numerical results are available in the Bioindustrial-Park GitHub repository, an official repository for complete biorefinery models and results to foster accessibility and deeper communication within the biorefinery simulation community. The repository also includes flowsheets, stream tables, utility requirements, design requirements, itemized costs, cash flow analysis, and reaction stoichiometries for each biorefinery. Detailed results of all biorefinery configurations are available in the Bioindustrial Park at https://github.com/BioSTEAMDevelopmentGroup/Bioindustrial-Park/blob/master/biorefineries/gas_fermentation/README.md. The full repositories can be downloaded directly from Github without the need to create an account. Alternatively, the biorefinery models can be installed using the command "pip install biorefineries==2.34.10" from your terminal (Mac/Linux) or command line (Windows) with a working Python 3.12 installation.

2.9 Uncertainty and Sensitivity

A total of 11 key economic and technological process performance parameters were explored via Monte Carlo simulations (Table S1 and Figure S2; SI). The lower bounds of distributions for fermentation performance parameters (e.g., productivity, titer, yield) represent near-term performance improvements relative to the current lab-scale performance and experimental findings in this study. The baseline assumptions reflect industry-ready assumptions on performance which can be attained with sustained research and development. The upper bounds are assumed to be the maximally attainable performance. Uniform distributions were chosen for all parameters given there is no data to suggest that any value is less attainable than another. These assumptions follow quantitative sustainable design methodology for the analysis

of new and conceptual technologies (Li et al., 2022). Latin hypercube sampling was used to generate 10,000 scenarios which were used to evaluate the full problem space. Halving the number of scenarios resulted in no significant change in uncertainty and sensitivity results. The sensitivity of the MSP and CI to each input parameter was characterized by Spearman's rank-order correlation, a measure of sensitivity between monotonic input and output parameters. Each contour plot was generated using a 10 x 10 grid of data points (100 scenarios evaluated for each contour plot). A Gaussian filter was applied to smooth discontinuities originating from automated discrete design decisions (e.g., number of fermenters in parallel).

The potential economic and environmental outcome was also evaluated under current fermentation performance assumptions. For the acetate-based configurations, a specific yield of 0.49 g / g DCW, a titer of 0.6 g / L, a productivity of 0.01 g / L / h, and a yield of 0.11 g alcohols / g acetate were assumed, consistent with the experimental findings of this study. For the glucose-based configurations, a specific yield of 1.50 g / g DCW, a titer of 1.6 g / L, a productivity of 0.016 g / L / h, and a yield of 0.126 g alcohols / g glucose were assumed, consistent with the experimental findings of Youngquist and coworkers (Youngquist et al., 2013b). These simulated scenarios are presented together with the uncertainty analysis to provide a reference to the current state of technology.

Results:

3.1 Δ*aceBAK* prevents biomass accumulation from acetate and improves yield

Acetyl-CoA is a central metabolic branch point with carbon flowing into either the TCA cycle for biomass and energy generation or into fatty acid biosynthesis for membrane components and product formation (Figure 2a). Flux into the TCA cycle is used to produce NAD(P)H for fatty acid biosynthesis, NADH for energy generation via oxidative phosphorylation, ATP via substrate level phosphorylation, and 4-carbon biomass precursors. These precursors are generated via the glyoxylate shunt pathway (at the cost of forfeiting one ATP and 2 reducing equivalents). Biomass accumulation via the glyoxylate shunt represents a significant pull on the acetyl-CoA pool, decreasing overall product yields. We stemmed the draw on acetyl-CoA towards competing pathways (i.e. biomass) by deleting the *aceBAK* operon which encodes the glyoxylate shunt pathway. Without the glyoxylate shunt, two molecules of CO_2 are generated for every acetyl-CoA molecule that enters the TCA cycle, and metabolites removed from the cycle for biomass generation cannot be replenished from acetate, limiting growth (Kornberg, 1966). To generate biomass and cultivate these strains, a secondary carbon source, such as glucose or glycerol, must be added to provide a source of C_4 units that offset biosynthetic draws from the TCA cycle. During production on acetate, decreased flux into the TCA cycle would result in increased acetyl-CoA availability for product synthesis. Distinguishing the end use for separate carbon sources as either biomass or bioproducts also allows simple control of growth and production stages via substrate feeding – mimicking a two-phase fermentation. Our bioprocess used glucose as the secondary carbon source because it enables carbon-efficient growth and ultimately accounts for a small portion of total carbon fed relative to acetate.

In a previous study by our group, a β-oxidation deficient *E. coli* strain was built to produce dodecanol from glucose by overexpressing three enzymes, a C_{12}-specific thioesterase ("BTE"), an acyl-CoA synthetase (^{Ec}FadD), and an acyl-thioester reductase (^{Ma}ACR) (Youngquist et al., 2013b) (Table 1). Here, the thioesterase siphoned fatty acid biosynthesis flux away from long-chain membrane precursors to dodecanoic acid. Without active β -oxidation, dodecanoyl-CoA, generated by FadD activity, accumulates and saturates ACR, catalyzing dodecanol synthesis. We integrated the dodecanol pathway genes into this β-oxidation deficient strain resulting in the base strain "JB36" (Table 1). We deleted the *aceBAK* operon in strain JB36 to obtain strain TAC58 (Table 1). We then compared the Δ*aceBAK* strain to its parent with the glyoxylate shunt intact by measuring their growth and oleochemical production in a 5 mL batch culture of minimal media with either solely glucose or glucose and acetate.

As expected, the strain TAC58 with the Δ*aceBAK* edit grew to the same OD on a mixture of glucose and acetate as it did on glucose, illustrating its inability to use acetate for biomass (Figure 2b). Conversely, the parent strain, JB36, grew to a higher OD on a mixture of glucose and acetate than on glucose alone, as some acetate is utilized to produce biomass. When both strains were fed glucose and acetate, TAC58 produced slightly lower fatty alcohol titers than JB36 but consumed significantly less acetate, resulting in an 82% higher product yield for TAC58 (Figure 2b-c). JB36 grew to a similar OD on acetate alone as when fed glucose and acetate but produced roughly one third of the dodecanol as the mixed feed. When compared to JB36 grown in a simple acetate-only process, TAC58 showed almost a 4x improvement in yield on an acetate basis, further demonstrating the benefit of preventing carbon loss to biomass. The yield improvement of removing *aceBAK* was consistent from 5 mL culture tubes to 50 mL baffled flask cultures, albeit with higher variability and slightly increased precursor accumulation

(data not shown). No glucose was detected in any of our 5 mL culture experiments, indicating that all strains consumed all of the glucose fed. We used the TAC58 production strain as a baseline for further metabolic engineering.

3.2 Integrating additional copies of BTE, ACR remove bottlenecks in terminal fatty alcohol pathway

Heterologous expression of a chain-specific acyl-ACP thioesterase is the first step to overproducing oleochemicals in *E. coli* (Jindra et al., 2023; Lennen and Pfleger, 2013, 2012; Su et al., 2024). Thioesterase expression must be optimized as extreme levels reduce growth, free fatty acid production, and cell viability (Lennen et al., 2011, 2010). Previously, our lab has demonstrated gram-per-liter dodecanol titers in *E. coli* when fed glucose by optimizing expression of the terminal fatty alcohol biosynthesis enzymes, which required integrating 3 copies of BTE in the genome, upregulating the native *E. coli* FadD, and introducing a plasmid expressing ^{Ma}ACR (Youngquist et al., 2013b). Acetate metabolism is unlikely to provide the same enzyme synthesis capability as glucose metabolism, so we explored the effect of gene copy number on pathway flux. Since the thioesterase has been shown previously to catalyze a key step to overproduce medium chain length oleochemicals by deregulating fatty acid biosynthesis from product inhibition, and enhanced expression, either from additional copies or solubility tags, has resulted in higher titers, and to ensure a sufficient supply of precursor for ACR, we started our strain engineering with 2 copies of BTE integrated (Jindra et al., 2023; Youngquist et al., 2013b). While plasmid-based expression can be a quick and tractable method of overexpressing a gene, our aim was to produce stable strains that could be used in an industrial process; therefore, we integrated ^{Ma}ACR into the genome to increase genetic stability and obviate the need for antibiotics, which are typically infeasible at scale. Therefore, we integrated different numbers of

BTE and ^{Ma}ACR expression cassettes into the TAC58 genome. Copies of BTE expression cassettes were integrated at the *fadE, fadAB*, and *fadK* loci (deleting the native loci genes involved in β-oxidation), and ^{Ma}ACR was integrated in the *ldhA* and *fadIJ* loci, which have previously been validated to support stable heterologous expression. We used a plasmid containing a BBR1 origin with an average copy number of ~5 per cell (Lennen et al., 2010) to provide an upper bound on ^{Ma}ACR expression. All genes were transcribed from heterologous P_{trc} promoter, including a swap of the native promoter for *E. coli*'s FadD, the acyl-CoA synthetase. We grew cultures in minimal media with a mixture of glucose (for biomass) and acetate (for product and energy). We measured titers, biomass (as OD600), and carbon consumption after 5 days of culture at 30°C.

When utilizing acetate for oleochemical production, no advantage was found to integrating 3 versus 2 copies of BTE when either one (SM018 compared to TAC58) or two (PP21 compared to PP20) ^{Ma}ACR expression cassettes were integrated (Figure 3a). Increasing ^{Ma}ACR copy number from one to two nearly doubled dodecanol titer and shifted the final product distribution from 54 (±1)% of total product as dodecanol to 83 (±1)% (Figure 3a). The increase in titer from two ^{Ma}ACR copies was accompanied by a relatively small increase in acetate consumption, resulting in a 1.8x increase in fatty alcohol yield from acetate (Figure 3b). Increasing to ~5 copies of ^{Ma}ACR via plasmid expression, however, did not increase total medium-chain oleochemical titer, and effected only a minor increase in conversion of free fatty acid intermediates to alcohols (Figure 3a). Given the aforementioned difficulties with plasmids during scale up and its lack of improvement over two genomic copies, we proceeded with the strain containing two copies of BTE and two copies of ^{Ma}ACR integrated in the genome, termed "PP20". The negligible benefits from additional copies of BTE (integrated) or ^{Ma}ACR (on a

plasmid) suggest that the expression of the final pathway enzymes was no longer the limiting step in converting acetate to dodecanol.

3.3 Acetate activation upregulation improves production

Having improved titers by upregulating the final enzymes in the fatty alcohol biosynthesis pathway, we sought to further increase production by increasing the acetyl-CoA pool. Intracellular acetate is activated to acetyl-CoA via one of two pathways in *E. coli* (Figure 4a). Acetyl-CoA synthetase (ACS) has a high affinity for acetate (K_m = 200 μM) but low V_{max} and catalyzes an irreversible route for acetate assimilation that proceeds through an acetyl-AMP intermediate (requiring 2 ATP to regenerate) (Brown et al., 1977; Castaño-Cerezo et al., 2009). It is subject to catabolite repression during excess glucose metabolism and is associated with growth on acetate in concentrations below 10 mM (Kumari et al., 1995). Acetate kinase (AckA) and phosphotransacetylase (Pta) have lower affinities for acetate (K_m = 7–10 mM) but high V_{max} and catalyze the reversible reaction to acetyl-CoA that proceeds through an acetyl-phosphate intermediate, requiring 1 ATP (Castaño-Cerezo et al., 2009). The two enzymes are constitutively expressed, and the direction of acetate assimilation or production is controlled thermodynamically by the level of extracellular acetate (Enjalbert et al., 2017). The AckA-Pta route is typically studied in the context of acetate production by *E. coli* in order to generate 1 ATP during overflow metabolism on glucose (Bernal et al., 2016).

Upregulating acetate activation to acetyl-CoA via overexpression of *E. coli*'s ACS or AckA-Pta has been demonstrated previously, but which route is beneficial varies. Some studies report benefits to upregulating ACS and/or detriments to upregulating AckA-Pta (Jo et al., 2019; Noh et al., 2018; Xu et al., 2018, 2017), while others report benefits to upregulating AckA-Pta (Chen et al., 2018; Huang et al., 2018; Li et al., 2019; Yang et al., 2020, 2019). Different

backgrounds of *E. coli* (e.g., K12 versus BL21) display different acetate production and consumption phenotypes based on reduced levels of ACS catabolite repression, and the unique biosynthetic pathway for each product influences how its production interacts with acetyl-CoA pools, the TCA cycle, and the rest of metabolism (Castaño-Cerezo et al., 2015). Furthermore, acetyl-phosphate plays a key regulatory role in *E. coli*, acetylating a broad range of proteins that influence acetyl-CoA pools, stress responses, and glucose metabolism; therefore, increasing flux through that node via AckA-Pta overexpression can trigger widespread metabolic changes (Castaño-Cerezo et al., 2015; Enjalbert et al., 2017; Schastnaya et al., 2023; Valgepea et al., 2010). In theory, the AckA-Pta pathway offers a more energy efficient route than ACS, but the complicated interplay of catabolite repression, regulation by acetyl-phosphate, culture conditions, and different branch points from central metabolism for different products make it difficult to predict the best route to upregulate in each use case. Ultimately, the tradeoffs of one route over the other can best be weighed empirically.

In addition, it has been reported that ACS of many prokaryotes, including *E. coli*, is post-translationally regulated by acetylation at lysine 609, which deactivates enzymatic activity (Bernal et al., 2014; Starai and Escalante-Semerena, 2004). A study of the ACS from *Salmonella enterica* showed that a point mutant, L641P, prevents this acetylation and thereby prevents deactivation (Starai et al., 2005). This mutant ^{Se}ACS has successfully been applied in *Saccharomyces cerevisiae* to increase acetate conversion to acetyl-CoA over native ^{Sc}ACS overexpression to increase production of acetyl-CoA-derived isoprenoids (Shiba et al., 2007), and overexpression of ^{Ec}ACS_L641P has been shown to increase acetate consumption in *E. coli* growing on mixed glucose and acetate medium (Novak et al., 2018); therefore, we included the deactivation resistant ACS(L641P) from *S. enterica* in our test.

We investigated if dodecanol production could be enhanced by accelerating the production of acetyl-CoA by integrating an additional copy of AckA-Pta or ACS from *E. coli* or a copy of the deactivation resistant mutant (L641P) from *S. enterica* into the chromosome under heterologous regulation (P_{Tet} promoter), creating strains PP22, PP23, and PP24, respectively. The native loci of *E. coli*'s *ackA-pta* and *acs* were unedited. We grew cultures in MOPS minimal media with a mixture of glucose (for biomass) and acetate (for product and some energy) and measured titers and carbon levels after 5 days. We tested two induction time points for the acetate uptake genes: induction at inoculation versus inducing after 24 h.

We found that inducing the upregulated acetate activation genes after 24 h has little impact on acetate consumption or oleochemical titer compared to the parent strain without upregulation (data not shown). Likely, since glucose is consumed within the first 24 hours, there was not a suitable carbon source to build significant amounts of new protein with, so induction of Δ*aceBAK* backgrounds while acetate is the sole carbon source is ineffective. When induced at inoculation, overexpressing ACS from *E. coli* in PP23 achieved a modest 12% boost in dodecanol titer (Figure 4b). The acetylation resistant mutant from *S. enterica* in PP24 resulted in a 16% improvement in dodecanol titer over the parent strain, and dodecanol comprised 90(±0.2)% of total oleochemicals compared to 84(±0.8)% in the parent strain. Interestingly, despite evidence that AckA-Pta upregulation can increase titers on acetate in some cases, it significantly reduced the titer of dodecanol in the case of PP22 (Figure 4b) (Kutscha and Pflügl, 2020). Since the genomic copy of *acs* is still present in the AckA-Pta upregulated strain, both pathways are likely expressed after glucose is depleted (removing catabolite repression of genomic *acs*), potentially forming or exacerbating a futile cycle of acetate formation by AckA-Pta and acetate assimilation by ACS and wasting 1 ATP in the process. Indeed, Novak et al.,

2018 observed a decrease in biomass yield when *E. coli* overexpressing ^{Ec}ACS_L641P were fed mixed glucose and acetate substrates, potentially due to an increased ACS-AckA-Pta cycle. However, we found that deleting the genomic *acs* in the AckA-Pta upregulated strain in fact further decreased titers and acetate consumption, suggesting that a futile cycle is not the mechanism for reduced titers (Supplemental Figure 3a-b). The ^{Ec}ACS upregulated strain with the genomic *ackA* deleted produced very little dodecanol and consumed no acetate, indicating that the ^{Ec}ACS is not responsible for acetate uptake in our conditions (Supplemental Figure S6a-b). Taken together with the increased titer in the ^{Se}ACS_L641P upregulated strain, these results suggest the ^{Ec}ACS is likely present in its deactivated and acetylated form and that the basal level of AckA-Pta expression in PP20 and the ^{Ec}ACS overexpression strain is better than over-expressed AckA-Pta. Finally, the ^{Se}ACS_L641P upregulated strain with the genomic *ackA* deleted produced modestly higher titers and yields than its counterpart with *ackA* intact or PP20 (Supplemental Figure 3a-b). This benefit is likely due to increased biomass by eliminating inefficient acetate production from glucose. While acetate activation through the ACS route costs more energy (and thereby reduces the maximum theoretical yield), AckA-Pta did not support high flux towards acetyl-CoA, and therefore we moved forward with the ^{Se}ACS mutant strain, "PP24", for bioprocess optimization. In sum, strain engineering efforts resulted in an improved yield on a total carbon basis from 0.035 ± 0.003 g alcohols / g total substrate in JB36 to 0.054 ± 0.001 g alcohols / g total substrate in PP24 before bioprocess optimization in bioreactors.

3.4 Bioreactor cultivation reaches high yield by bolus feeding acetate

After we increased flux to dodecanol by overexpressing the terminal fatty alcohol pathway and substrate activation enzymes, we tested our improved strain's performance in controlled bioreactors which provide the benefits of pH control, aeration, and tunable feeding

strategies. The previous small-scale production cultures were supplied 2 g/L glucose and grew to low cell densities (OD ~1.5). We sought to increase biomass in order to maximize volumetric productivity during scale up to 500 mL cultures by supplying additional glucose at 4, 8, and 12 g/L, leveraging the 2-stage fermentation method with distinct carbon sources for growth and production enabled by the *aceBAK* deletion. Unexpectedly, we found supplying initial glucose beyond 4 g/L drastically shifts the final product distribution towards dodecanoic acid with almost no fatty alcohols in terminal measurements (Figure S4a). Time course data shows most of the fatty acids are produced after glucose is depleted, indicating that the effect of cells experiencing higher glucose concentrations during the growth stage impacts the production stage despite glucose not being present (Figure S4b-d). Feeding glucose in boluses to maintain glucose concentrations below ~6 g/L while still providing higher cumulative amounts of glucose resulted in the same product shift towards predominantly dodecanoic acid (Figure S7a-d). Therefore, we used 4 g/L initial glucose in our bioreactor runs to generate sufficient biomass without incurring unfavorable product distributions.

Finally, we compared different acetate feeding strategies: a pH-controlled glacial acetic acid feed (pH-stat) versus bolus additions of concentrated sodium acetate. Fermentations of PP24 in bioreactors comprised a growth stage on glucose wherein the media becomes acidified (and the bioreactors add base to maintain the set pH), followed by a production stage that consumes acetate and makes the culture more basic (again, the bioreactors add acid to maintain the pH). When acetic acid is used as a pH control, acetate levels stayed relatively constant throughout the fermentation as acetate is consumed and replaced by acetic acid (Figure 5c). Due to catabolite repression, acetate is not consumed significantly until glucose is depleted (Figure 5c-d). Cultures were induced when dissolved oxygen fell below 60%, roughly 10-15 hours after inoculation and

2-4 hours before glucose is depleted. This method coordinates induction at similar growth stages across replicates and provides sufficient time and usable substrate (i.e., glucose) to synthesize the induced fatty alcohol pathway and ^{Se}ACS genes while ensuring that the majority of the glucose is used to generate biomass with minimal oleochemical products synthesized from glucose.

Acetic acid-fed pH-stat cultures and bolus-fed cultures produced a similar amount of oleochemicals (Figure 5a). Acetic acid consumption measurements were highly variable for pH-stats, potentially due to the method of weighing acetic acid feed bottles at the beginning and end of the experiment, making comparisons of yield between the feeding strategies difficult (Figure 5b). If acetate consumption is higher in pH-stat cultures without a proportional increase in titer and no additional biomass, then the data would imply that more acetate is being converted to CO_2 and results in lower yields (Figure 5b). In a previous study, it was shown that *E. coli* primarily funnels carbon from glucose into biomass, products, CO_2, or acetate, supporting the conclusion that additional acetate consumption without increased product or biomass would likely end up as CO_2 (Youngquist et al., 2013b). Acetate concentrations above 5 g/L have been ghhhreported to inhibit growth (Chong et al., 2013); therefore, maintaining acetate concentration at 5 g/L, while not above the inhibitory concentration, may still trigger acid stress responses that consume energy and increase acetate consumption without increasing flux towards products. Acetic acid-fed cultures achieved an average of ~950 (±130) mg/L of total oleochemicals with 67 (±2)% as dodecanol. Bolus-fed cultures, on the other hand, produced an average of 740 (±68) mg/L of total oleochemical products, qualitatively but not statistically lower than pH-stats (p-value = 0.069), with 75 (±11)% as dodecanol (Figure 5a). Interestingly, in both feeding methods, roughly half of the total dodecanol was produced between 16 hours (when glucose was depleted) and 48 hours, after which dodecanol production slowed (Figure S6a-b). Dodecanoic acid began

to accumulate after 72 hours, indicating a mismatch in rates between dodecanoic acid production and the subsequent acyl-CoA production and reduction to dodecanol. This could be a result of faster ^{Ma}ACR enzyme degradation than BTE degradation, or a decrease in the NADPH pool used by ^{Ma}ACR as cells shift into stationary phase.

Finally, a fed-batch fermentation of PP24 achieved an average yield of 0.11 ± 0.018 g fatty alcohols/g acetate compared to 0.06 ± 0.024 g fatty alcohols/g acetate in the pH-stat (Figure 5b). These yields represent 37% of the maximum theoretical yield in the bolus-fed case and 20% of maximum theoretical yield in the pH-stat, compared to only 13% in the initial JB36 strain, demonstrating that metabolic engineering and fermentation optimization strategies led to an overall ~2.8-fold increase in yield of fatty alcohols from acetate. While glucose is an unfavorable feedstock from an environmental and economic perspective, bolus-fed cultures consumed an average of 2.5g of acetate compared to 2g of glucose, and longer fermentations should increase this ratio as more acetate is fed, showing promise for acetate utilization for product synthesis and energy to outweigh the drawbacks of glucose used for biomass generation. Fermentation metrics like oleochemical yield (g dodecanol/g acetate) and specific yield (g dodecanol/g DCW) from our final bioreactor fermentation were used in the TEA and LCA models to evaluate tradeoffs in feeding glucose versus acetate for cell growth and determine where our process fits in the opportunity landscape.

3.5 Opportunity for market competitiveness and improved environmental impact

TEA and LCA were used to identify conditions under which the proposed process would be economically and environmentally sustainable. We used TEA and LCA to investigate the competitiveness of the proposed bioprocesses against fossil fuels, determine which assumptions

and parameters are most important for market competitiveness, and evaluate the trade-offs between the different configurations. Under the current experimental performance assumptions, all configurations resulted in MSPs and CIs greater than market price (5 USD·kg^{-1}) and CI of fossil fuel-based routes (2.97 kg·CO_2eq·kg^{-1}), respectively (Figure 6). However, the fermentation processes are early-stage technologies with large room for potential improvements assuming continued research and investment. We conducted a Monte Carlo uncertainty analysis to characterize the opportunity space over a range of assumptions on future technological performance (yield, titer, productivity) as well as on other key parameters such as processing capacity and H_2 price. The Monte Carlo uncertainty analysis resulted in a large opportunity space for the acetate-based configurations to have a lower environmental impact than fossil fuel routes and become market competitive (Figure 6a). The glucose configuration, however, resulted in a large fraction of simulated scenarios having greater carbon intensity than fossil fuel rounds. Overall, simulated scenarios demonstrated environmental benefits of the acetogen-coupled fermentation to the fossil fuel-based alternative, with the acetate configuration having the lowest potential environmental impact and the acetate/glucose-seed configuration having the best potential economic viability.

The acetate configuration, which diverts a fraction of the bioreactor substrate to grow the seed, resulted in a CI of -1.03 [-1.69, 0.24] kg·CO_2eq·kg^{-1} (presented as median [5th, 95th] percentiles) with all simulated scenarios having a CI lower than the estimated CI of fossil-based routes (2.97 kg·CO_2eq·kg^{-1}) and even lower than the estimated CI of palm kernel oil-based routes (5.27 kg·CO_2eq·kg^{-1}). Converting acetate to dodecanol and feeding glucose to grow the seed resulted in a CI of 0.519 [-0.916, 4.393] kg·CO_2eq·kg^{-1}, with 88% of simulated scenarios having a lower CIs compared to fossil-based routes. Directly fermenting glucose to dodecanol

resulted in a CI of 4.2 [1.8, 9.13] $kg \cdot CO_2eq \cdot kg^{-1}$, with only 24% of scenarios having lower CIs compared to fossil-based routes. Therefore, an integrated acetate-to-dodecanol production process that leverages flue gas as the carbon source can potentially have more environmental benefits compared to using glucose, depending on the fermentation performance (i.e., titer, rate, and yield). These results stem from how glucose production can be a carbon intensive process due to harvesting, transportation, and biorefining activities.

Between the two acetate-based configurations, the acetate/glucose-seed configuration resulted in greater economic potential (MSP of 5.61 [3.36, 9.56] $USD \cdot kg^{-1}$) compared to the acetate configuration (MSP of 6.4 [3.66, 11.61] $USD \cdot kg^{-1}$). The high specific yield of glucose (0.45-0.50 $g_{DCW} \cdot g_{glucose}^{-1}$) compared to acetate (0.30 $g_{DCW} \cdot g_{acetate}^{-1}$; Rabbers et al., 2022; Shiloach and Fass, 2005) makes glucose an effective substrate for cell mass production. The relative viability of the configurations depended on the specific prices of H_2 and glucose. Under baseline assumptions, the hydrogen price must be as low as 2.45 $USD \cdot kg^{-1}$ for the acetate configuration to be more economic than the acetate/glucose-seed configuration. Because economics is the main bottleneck to commercial deployment and achieving a H_2 price lower than 2.45 $USD \cdot kg^{-1}$ may not be feasible in the near horizon, the acetate/glucose-seed configuration may be the more advantageous option. The glucose configuration resulted in an MSP of 4.71 [2.68, 8.34] $USD \cdot kg^{-1}$, which is lower, but comparable to the acetate/glucose-seed configuration (5.61 [3.36, 9.56] $USD \cdot kg^{-1}$). This result demonstrates that the integrated bioprocess may result in environmental benefits with similar market outcomes compared to glucose-based pathways.

Among all the process performance parameters, both the economic and environmental sustainability are most sensitive to the oleochemical bioreactor yield, as determined by the sensitivity analysis (Figure 6b and d). The hydrogen price is the second most impactful

parameter driving economics. While the current price of hydrogen has been estimated to be within 5 to 6 USD·kg^{-1}, the price of hydrogen is expected to fall within 2 to 4 USD·kg^{-1} assuming improvements to wind and solar power and proton exchange membrane electrolysis technologies[14,15]. To further characterize the impact of future improvements to these key technologies, we evaluated the MSP across potential oleochemical yields and hydrogen prices (Figure 6c). Minimally, the bioreactor yield for the glucose-seed train configuration needs to be improved to 51–78% of the theoretical maximum (depending on the hydrogen price) to meet the market price for the acetate/glucose-seed configuration and 55–98% for the acetate configuration (Figure S5). These ranges provide critical targets for research and technological development.

Improvements to the specific yield (in $g_{product}/g_{cell}$) of the oleochemical bioreactor may also greatly improve the economic and environmental sustainability of the process by reducing the amount of carbon needed to generate seed biomass, assuming a constant production capacity (Figure 6b and d). Improving other fermentation performance parameters (e.g., bioreactor titers and productivities) would also have a positive impact on the economic and environmental sustainability to a lesser degree. In this process, the acetate titer plays a lesser role because the dilute effluent from the acetate bioreactor can be fed directly to the oleochemical bioreactor. The process is also less sensitive to the oleochemical titer because the oleochemical is secreted extracellularly which allows for easy recovery by solvent extraction; in contrast to the distillation-based separation of small-molecule alcohols and organic acids. The impact of titer, productivity, and yield on the MSP and CI across all configurations is further characterized in Figures S3–S4 to guide strain developers to work towards optimal improvements for economic and environmental sustainability.

One key bottleneck of the process design is mass transfer limitations of CO_2 and H_2 at the acetate air-lift bioreactor. At a high height-to-diameter of 12 for all bioreactors, 11 % of hydrogen and 12 % of carbon fed to the acetate bioreactor cannot be transferred to the liquid phase due to mass transfer limitations. This bottleneck stems from sparging air (79 vol % N_2) to the oleochemical bioreactor which results in a low concentration of CO_2 recycled to the acetate bioreactor (20.1 wt. % CO_2). Design configurations which maximize CO_2 concentrations, such as employing carbon capture at the oleochemical bioreactor gas vent, would improve H_2/CO_2 uptake and minimize capital/operating costs of the bioreactors and auxiliary compressors. Alternatively, green hydrogen production via the electrolysis of water also generates O_2, potentially enabling oxygen sparging as a strategy to aerate the oleochemical bioreactor while generating a concentrated CO_2 recycle stream for the air-lift bioreactor. Future TEA/LCA studies may seek to optimize the production pathway by assessing the different design alternatives. One key assumption in this study is that green hydrogen is readily available for up to 80 $MT \cdot yr^{-1}$. However, there may be variability in hydrogen supply due to the inherent uncertainty in the renewable energy supply used to power water electrolysis and the high cost of hydrogen storage, and therefore additional capital cost may be incurred for operationally flexible designs. Future TEA/LCA studies with integrated supply chain analysis considering renewable electricity supply and green hydrogen storage may seek to optimize designs for operational flexibility.

4.1 Discussion:

The decrease in acetate consumption caused by the *aceBAK* knockout led to increased yields, but the greater acetate consumption in the parent strain, JB36, illustrates the potential of cells to process acetate when there is a strong enough draw on the acetyl-CoA pool, like that from biomass generation. We have upregulated the terminal fatty alcohol production pathway,

749 but the resulting strain still did not consume as much acetate as JB36, suggesting that there is still
750 potential for increased flux through acetyl-CoA. Directly upregulating the enzymes that convert
751 acetyl-CoA into downstream metabolites for fatty acid biosynthesis, e.g., the acetyl-CoA
752 carboxylase complex (ACC, encoded by *accABCD*) could mimic the pull on the acetyl-CoA pool
753 normally created by growth; indeed deregulating or improving activity of the ACC has been
754 shown to increase availability of malonyl-CoA and production of downstream products (Lai et
755 al., 2021; Wu et al., 2021; Zha et al., 2009).

756 The TCA cycle generates one NADPH for every two NADH, but the pathway to
757 dodecanol consumes two more NADPH than NADH due to ^{Ma}ACR's specificity for NADPH.
758 Other studies that produce target chemicals from acetate with similar cofactor imbalances have
759 reported benefits in titer from increasing NADPH pools via deregulation of the transhydrogenase
760 *pntAB* or overexpressing it alongside the NAD kinase, *nadK* (Li et al., 2021; Song et al., 2018;
761 Yang et al., 2020; W. Zhang et al., 2025). Similarly, extra reducing equivalents could be supplied
762 by feeding ethanol instead of acetate, which acetogens can overproduce, although any benefits
763 must be weighed against the cost of consuming additional H_2.

764 While we showed that a heterologous and deregulated ^{Se}ACS(L641P) increased titers and
765 yields of dodecanol, and upregulation of AckA-Pta did not, the energy savings of the latter
766 pathway motivate further exploration. We have only tested the AckA-Pta upregulated strain at
767 the 5 mL scale, but the pH-stat method of acetic acid feeding in bioreactors offers a convenient
768 way to test optimal extracellular acetate concentrations to drive the AckA-Pta reaction in the
769 assimilation direction without a decrease in acetate over time. As only 2 ATP, 2 NADH, and 1
770 NADPH are generated from each acetyl-CoA that enters the TCA cycle, expending only 1 ATP
771 instead of 2 to activate acetate represents a considerable step towards the maximum theoretical

yield if the AckA-Pta route can be utilized. Ultimately though, high flux through the acetyl-phosphate node could affect protein acetylation with detrimental effects throughout metabolism (Schastnaya et al., 2023), motivating investigating energy savings elsewhere in metabolism. For example, cellular machinery that is not used or not desired in industrial bioreactors, like flagella or stress response proteins, could be deleted to reduce unnecessary carbon and energy requirements (Youngquist et al., 2017). Similarly, reducing the genome of *E. coli* to eliminate unnecessary genes has been shown to improve production in some stressed environments, purportedly by diminishing the strains' maintenance energy (Cordell et al., 2024, 2023).

Our TEA model showed that generating biomass from glucose is economically more favorable than acetate-fed seeds due to high H_2 costs (at present) and the higher biomass yield of *E. coli* on glucose. As technological progress decreases H_2 prices or alternative waste streams are employed that contain higher ratios of reduced compounds than our model considers, growing cells on acetate may become economically feasible. In these cases, conditional knock outs or dynamic metabolic control could be applied to disable the *aceBAK* operon and transition to the production stage, enabling growth on acetate during the initial stage while still gaining the benefits in yield from reduced flux to biomass demonstrated in this work (Soma et al., 2014; Ye et al., 2021). The transition from growth to production stage is usually triggered by nutrient depletion, but few reports describe nutrient limitation effects in *E. coli* under acetate metabolism (rather, glucose or glycerol are used as substrates), highlighting an open area of investigation to accelerate acetogen-coupled bioprocess development (Li et al., 2018; Shimizu, 2013).

The techno-economic and life cycle analyses demonstrated the potential environmental benefits and market viability of the proposed bioprocess compared to both conventional fossil-based routes and the alternative glucose-based pathway. There are, however, a wide range of

alternative routes. Among biomass-based pathways, integrated 1G/2G production pathways cofermenting non-structural sugars together with cellulosic sugars (e.g., sugarcane juice and bagasse, corn starch and corn fiber) has been shown to have improved economic and environmental outcomes (Iram et al., 2022; Pinheiro et al., 2025). More recently, engineered oil crops such as oil-cane and oil-sorghum may provide a sustainable source of triacyl glycerides that can serve as a precursor for fatty alcohol production (Cortés-Peña et al., 2024; Park et al., 2025). Within flue gas-based pathways, small molecules such as ethanol can be produced from flue gas as a substrate for oleochemical production (Herwig et al., 2020; Hu et al., 2016). Lastly, acetate and ethanol may also be produced by electrosynthesis (among other renewable routes). It is unclear how these production pathways compare and what developments are required to achieve market viability and reduced carbon footprints. There is a need for broader TEA/LCA studies which systematically characterize the trade-offs/advantages of each alternative pathway, prioritize the development of key technologies, and establish critical targets for sustainability. To this end, the open-source bioprocess models developed in this study may be leveraged in future studies to compare with alternative production routes.

4.2 Conclusion

The aim of this work was to use metabolic and fermentation engineering strategies in *E. coli* to pave the way for an industrially viable and sustainable route to oleochemicals. In this integrated technoeconomic and metabolic engineering study, we demonstrated the concept with conversion of acetate to dodecanol. Through deleting the *aceBAK* operon, we demonstrated the benefit of reduced biomass flux and the advantage of distinct carbon sources on process control for two-stage fermentations. We balanced BTE and ^{Ma}ACR expression to maximize flux from acetate

towards dodecanol and found the best ratio of genes was different than when dodecanol is produced from glucose. This finding emphasizes the importance of testing metabolic engineering techniques in a process that most closely resembles potential downstream applications. Applying our improved strains in a controlled bioreactor with bolus-fed acetate, we achieved ~550 mg/L of dodecanol and 740 mg/L of total oleochemicals. More importantly for the economics of our process we improved the yield of fatty alcohols on acetate almost 3-fold to reach 37% of the theoretical maximum. Our TEA showed that at 51% of the theoretical maximum yield, our process becomes cost competitive with fossil fuel-based routes. Furthermore, LCA showed that our acetogen-coupled bioprocess significantly reduces the environmental impact (measured as CI) of dodecanol production and can even reach a negative CI, representing a promising contribution towards a circular bioeconomy. While this study focused on a single oleochemical product, we hope our results illustrate the potential of acetate for sustainable biomanufacturing and motivate analogous studies to demonstrate other biomanufacturing processes using acetate as a feedstock.

Acknowledgements:

The authors would like to thank our collaborators at LanzaTech, especially Vicki Liu, Sean Simpson, Michael Koepke, Chad Henry, Wayne Mitchell, Marilene Pavan, Nick Fackler, and Daniel Payan for their valuable conversations and contributions, even if they could not be included in the manuscript.

Funding Sources:

The information, data, or work presented herein was funded in part by the Advanced Research Projects Agency—Energy (ARPA-E), U.S. Department of Energy, under Award Number DE-

AR0001503. TAC was supported by an NHGRI training grant to the Genomic Sciences Training Program, Award Number 5T32HG002760.

Figures and Figure Captions:

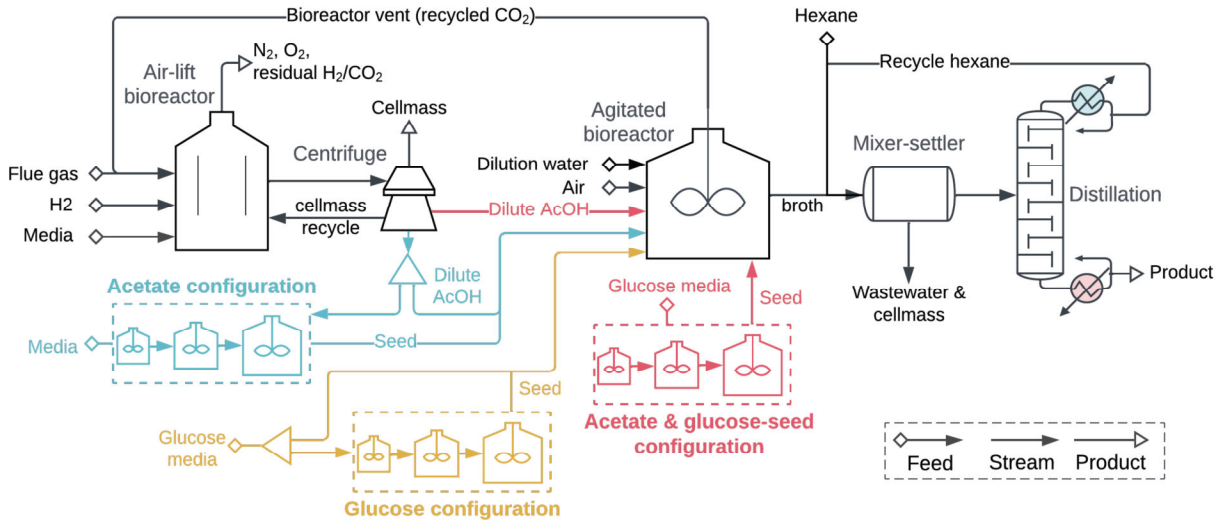

Figure 1. Simplified process flow diagram of the CO_2/H_2 to oleochemical production process, including acetate production, seed trains, and oleochemical production. Wastewater treatment and utility production systems, including the on-site boiler and turbogenerator, are omitted for simplicity.Unit operations specific to the acetate (blue), acetate/glucose-seed (red), and glucose (yellow) configurations are color coded.

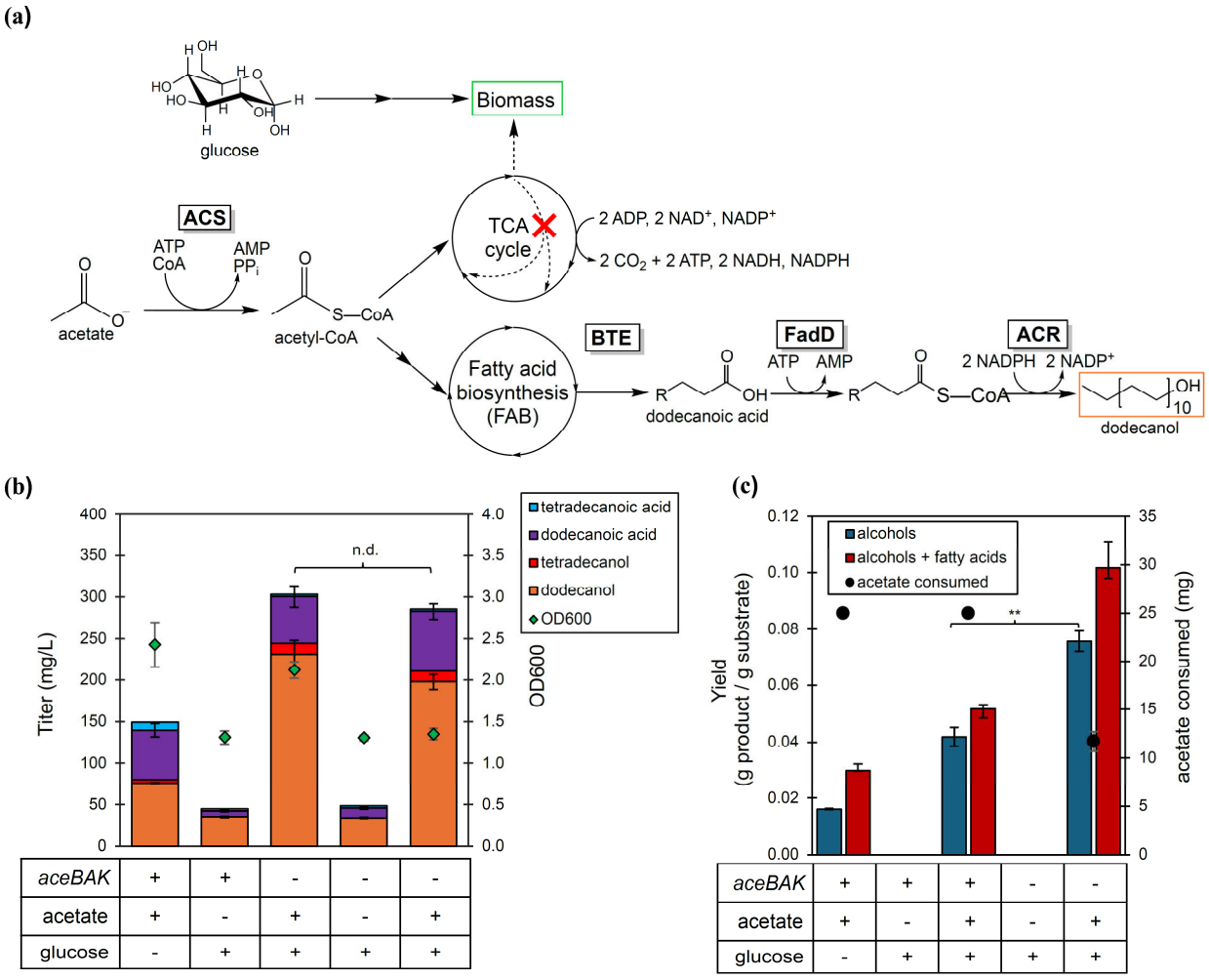

Figure 2. Deletion of *aceBAK* prevents biomass generation from acetate and increases yield. **(a)** Pathway from acetate to dodecanol, with a branch point at acetyl-CoA for carbon to either enter the TCA cycle for energy and biomass generation or fatty acid biosynthesis for membrane components and product generation. Two heterologous enzymes, BTE and ACR are integrated on the chromosome, and a heterologous P_{Trc} promoter is integrated to replace *E. coli*'s native FadD promoter. Deleting the *aceBAK* operon prevents accumulation of biomass from acetate, necessitating a secondary non-C2 carbon source: glucose is shown. **(b)** Final titers (bars) and ODs (green diamonds) after 5 days for 5 mL cultures in MOPS minimal media with a 10% dodecane overlay fed either 5 g/L acetate, 2 g/L glucose, or both. Error bars represent the

standard deviation of 3 biological replicates. **, statistically significant difference in dodecanol titers, α=0.01 **(c)** Acetate consumption (black circles) and yields (bars) on acetate for C12 and C14 alcohols or C12 and C14 alcohols + C12 and C14 fatty acids. For cases where both glucose and acetate were fed, titers from cultures only fed glucose were subtracted to estimate the amount of product from acetate alone. Error bars represent standard deviation of 3 biological replicates.**, statistically significant difference in alcohol yields, α=0.01.

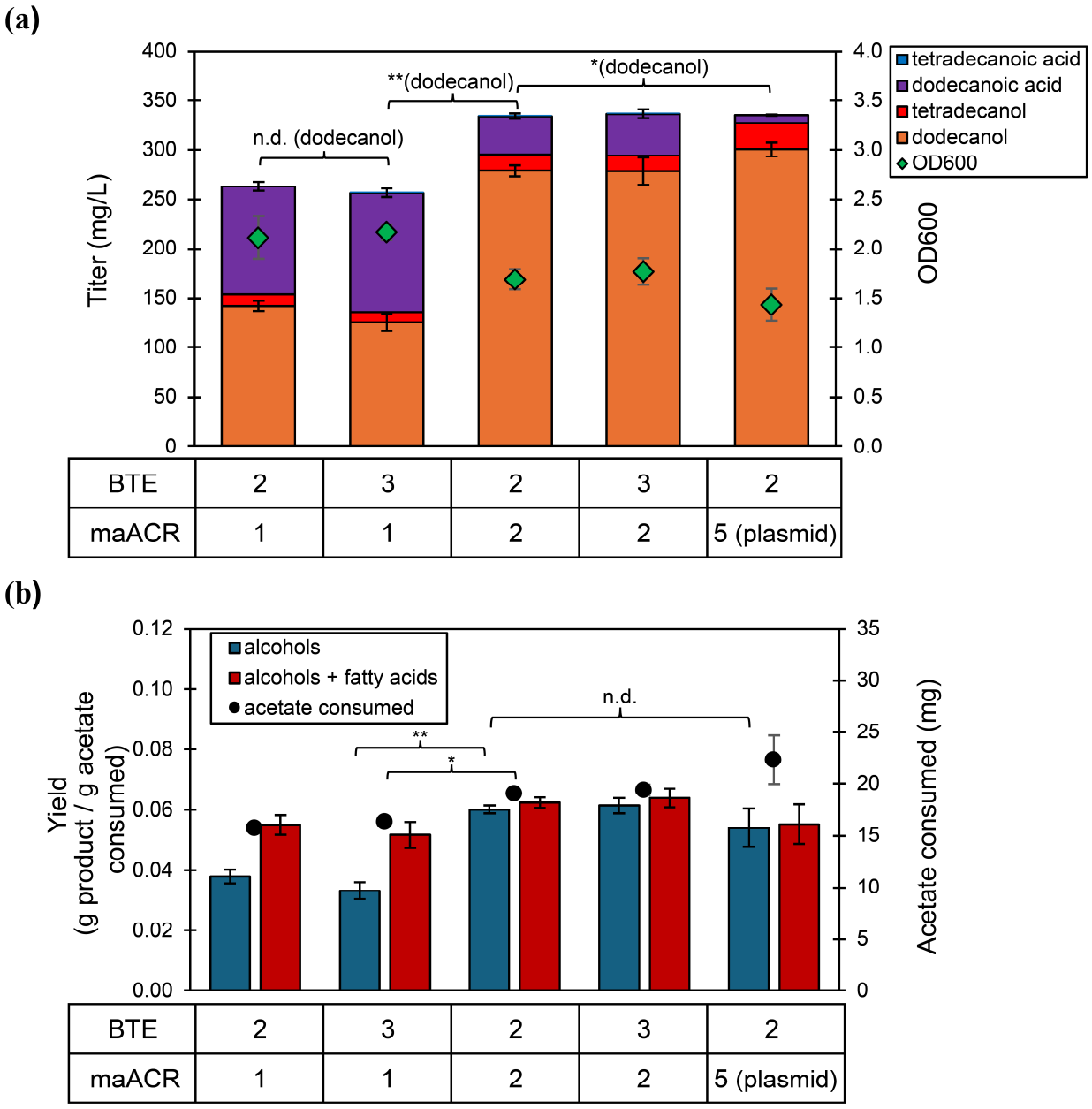

867

868 **Figure 3.** 2 copies of BTE and 2 copies of maACR provide optimal flux to dodecanol. **(a)** Final
869 titers (bars) and ODs (green diamonds) after 5 days for 5 mL cultures in MOPS minimal media
870 with a 10% dodecane overlay and 2 g/L glucose, 5 g/L acetate. X-axis chart displays number of
871 copies of each gene integrated into the chromosome, except for the "Plasmid" case using a BBR1
872 backbone. Error bars represent standard deviation of 4 biological replicates. n.d., no statistical
873 difference in dodecanol titer using ANOVA *, statistically different dodecanol titer, α=0.05; **,

874 statistically different dodecanol titer, α= 0.01. **(b)** Acetate consumption (black circles) and yields
875 (bars) on acetate for C12 and C14 alcohols or C12 and C14 alcohols + C12 and C14 fatty acids.
876 For cases where both glucose and acetate were fed, titers from cultures only fed glucose were
877 subtracted to estimate the amount of product from acetate alone. Error bars represent standard
878 deviation of 4 biological replicates. "*" or "**", statistically different acetate consumption or
879 alcohol yield, α= 0.05 or α=0.01, respectively.
880

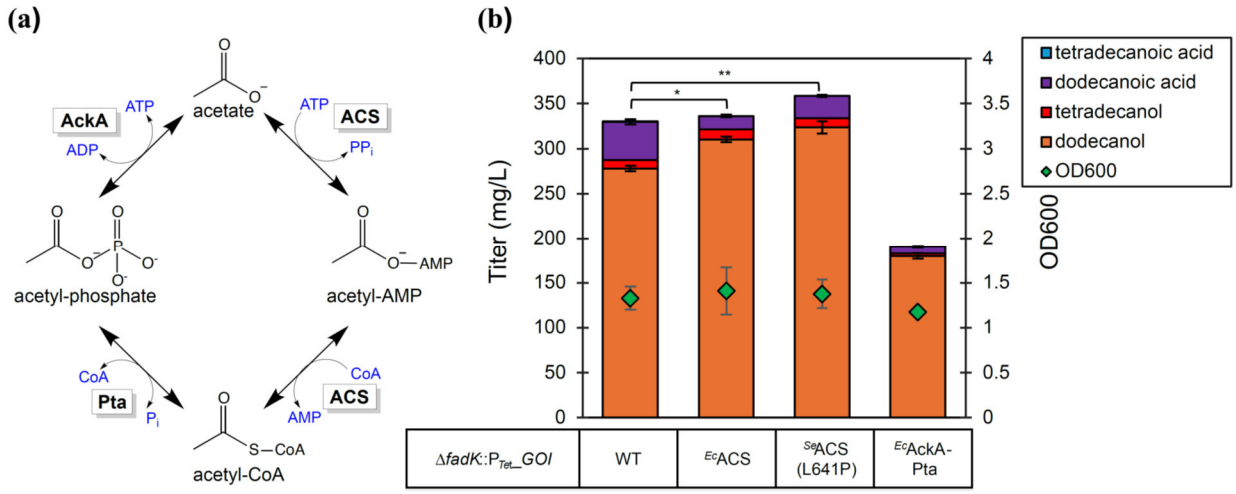

881

882 **Figure 4.** Overexpressing a mutant of the ACS from *Salmonella enterica* increases dodecanol

883 titer. a) The two native routes to acetyl-CoA from acetate in *E. coli*. b) Final titers (bars) and

884 OD600s (green diamonds) after 5 days for 5 mL cultures in MOPS minimal media with a 10%

885 dodecane overlay, 5 g/L acetate and 2 g/L glucose. Upregulated genes were integrated into the

886 *fadK* locus in *E. coli* under control of the P_{Tet} promoter. Error bars represent the standard

887 deviation of 4 biological replicates. "*" or "**", statistically different dodecanol titers, $\alpha = 0.05$

888 or $\alpha = 0.01$, respectively.

889

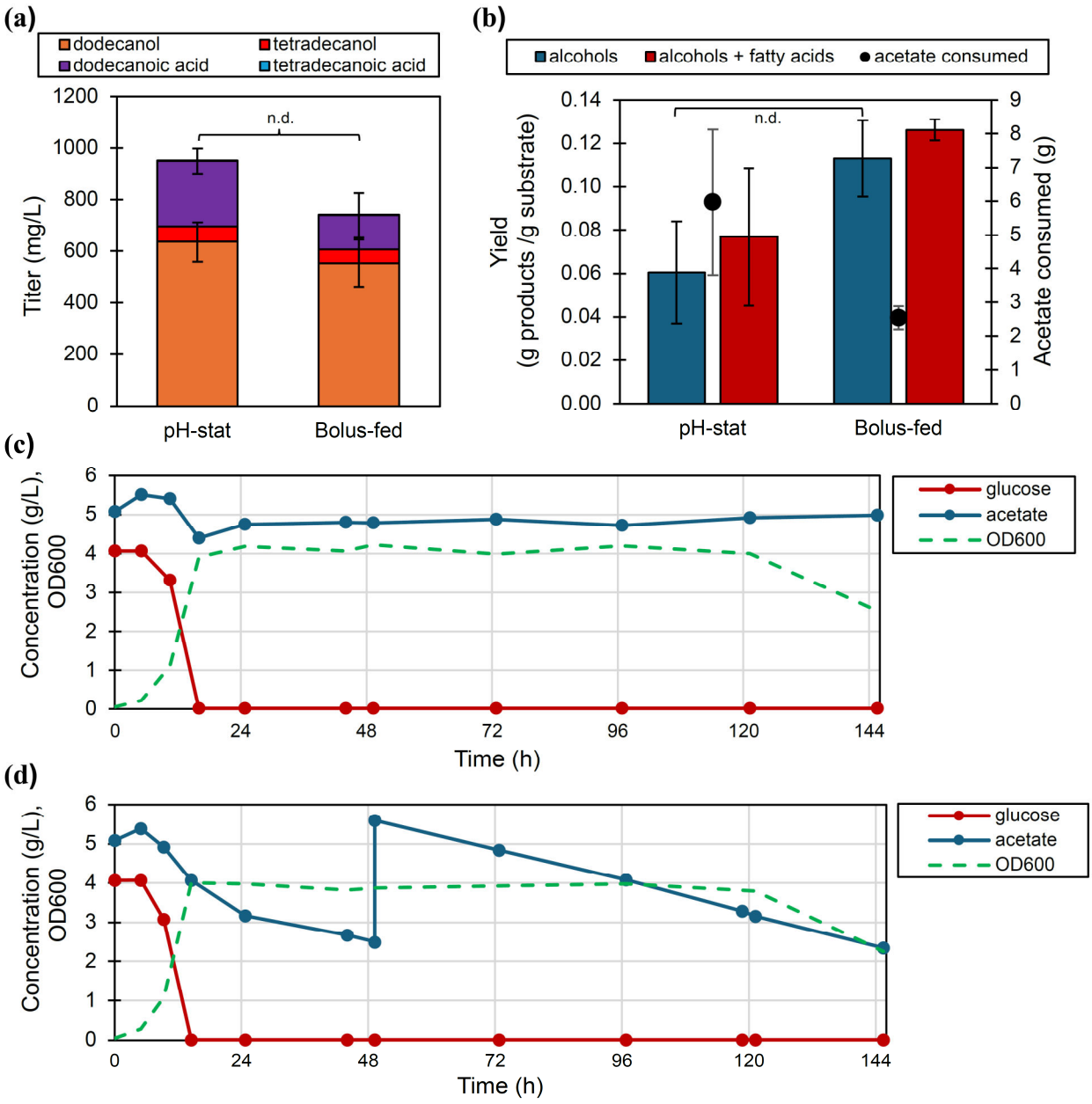

Figure 5. Controlled bioreactor fermentation results in improved yields **(a)** Final titers (bars) and OD600s (green diamonds) after 6 days for 500 mL cultures of PP24 in MOPS minimal media with a 10% dodecane overlay, 4 g/L glucose and variable amounts of acetate in 1 L stirred bioreactors. Error bars represent standard deviation of 3 biological replicates. **(b)** Acetate consumption (black circles) and yields (bars) on acetate for C12 and C14 alcohols or C12 and C14 alcohols + C12 and C14 fatty acids. To determine product from acetate alone, the titer at the

time point corresponding to glucose depletion was subtracted from the end titer. Acetic acid consumption in pH-stat cultures was determined by weighing acetic acid bottles before and after fermentation, using a non-feeding bottle as a control to account for evaporation, which may contribute to variability. Error bars represent standard deviation of 3 biological replicates. n.d., not statistically different. Representative single-bioreactor plots showing OD600, acetate concentration (g/L) and glucose concentration over the course of 144 h cultivations for PP24 in **(c)** a pH-stat fed acetic acid or **(d)** a bioreactor fed boluses of concentrated Na^+acetate. Additional replicates are reported in Supplemental Figure S7.

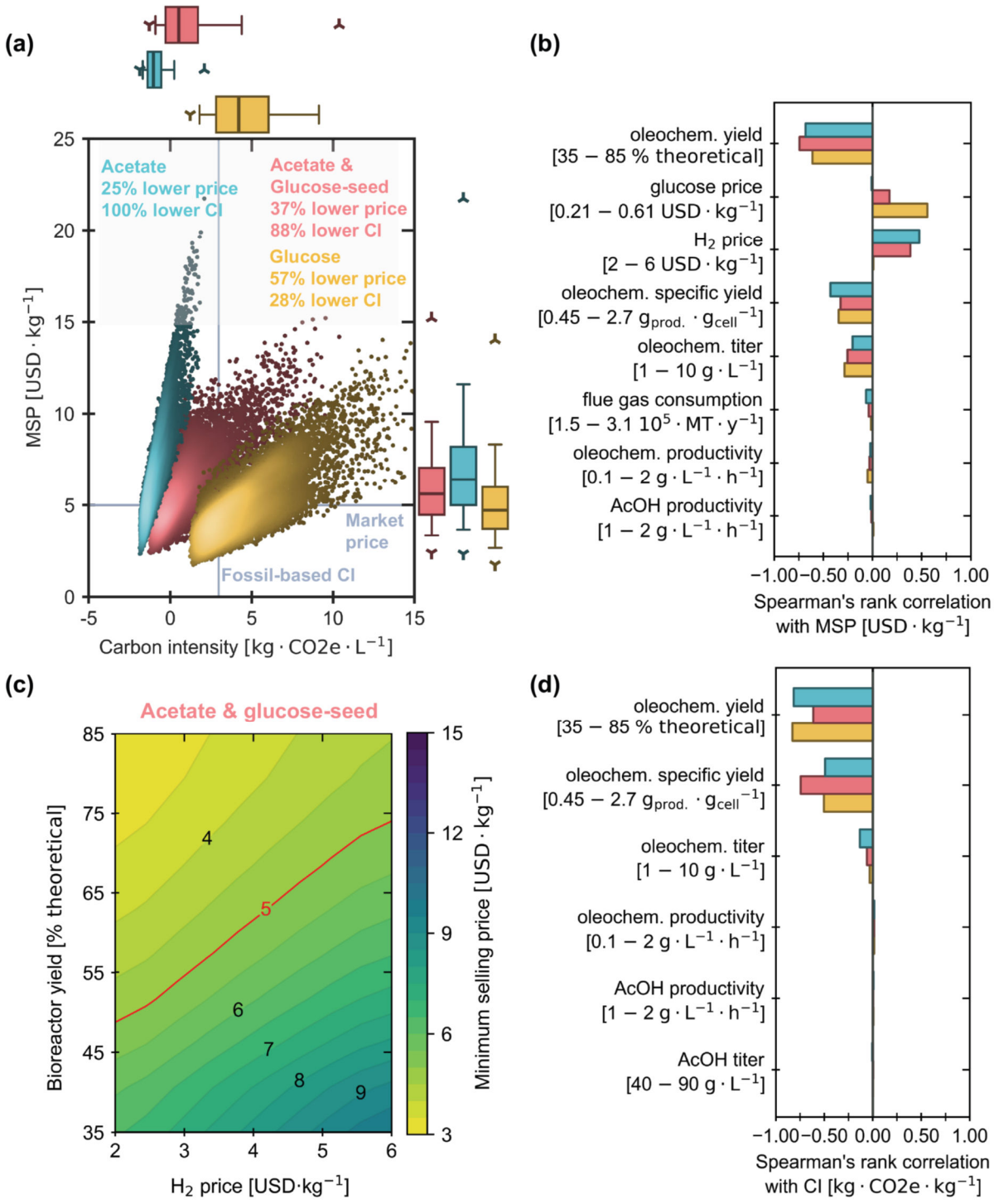

906

907 **Figure 6. (a)** Scatter plot of the MSP and the CI of dodecanol under uncertainty for the acetate

908 (blue), acetate/glucose-seed (red), and glucose (yellow) configurations. Experimental

909 performance scenarios are represented as stars. The box and whisker plots of the dodecanol yield

and the carbon intensity represent median values (dark, solid lines), 25th–75th percentiles (shaded region), 5th and 95th percentiles (whiskers), and minimum and maximum values (triangles). The horizontal line represents the upper bound of the market price for dodecanol (5 $USD \cdot kg^{-1}$). Thus, relative to the market price of dodecanol, simulated scenarios below the horizontal line can be market competitive. The vertical line represents the estimated CI for dodecanol produced from fossil fuel pathways (2.97 $kg \cdot CO_2eq \cdot kg^{-1}$). Simulated scenarios to the left of the vertical line achieved a lower environmental impact. **(b)** Sensitivity of the MSP of the glucose-fed and acetate-fed seed train configurations to parameters varied in the Monte Carlo simulations, as determined by Spearman's rank correlation coefficients (ρ). **(c)** Contours of the MSP across H_2 price (x-axis) and oleochemical yield (y-axis) for the acetate/glucose-seed configuration under baseline assumptions shows how bioreactor yields above 48% are needed to meet the market price. **(d)** Sensitivity of the CI to parameters varied in the Monte Carlo simulations, as determined by Spearman's rank correlation coefficients (ρ). For both MSP and CI sensitivities, only parameters with $|\rho| > 0.01$ are shown. Each parameter is modeled as uniform distributions. The minimum and maximum values for each parameter are listed in brackets.

Author Contributions:

Name	Current Email	Affiliation	Contribution
Paul M. Perkovich	pmperkovich@gmail.com	UW-Madison	Investigation, Methodology, Formal analysis, Visualization, Writing – original draft
Yoel R. Cortés-Peña	Cortespea@wisc.edu	UW-Madison	Investigation, Software, Methodology, Visualization, Writing – original draft
Justin J. Baerwald	Jbaerwald@berkeley.edu	UW-Madison	Methodology
Thomas H. Graupmann	Thgraupmann@gmail.com	UW-Madison	Investigation
Theodore A. Chavkin	Tchavkin@wisc.edu	UW-Madison	Methodology (strain creation)
Shivangi Mishra	Smishra47@wisc.edu	UW-Madison	Investigation
William T. Cordell	Wcordell@nrel.gov	UW-Madison	Methodology
Victor M. Zavala	victor.zavala@wisc.edu	UW-Madison	Methodology, writing-review and editing
Brian F. Pfleger*	brian.pfleger@wisc.edu	1. UW-Madison	Conceptualization, funding acquisition, formal analysis, writing-review and editing

References:

Barbose, G., 2024. U.S. State Renewables Portfolio & Clean Electricity Standards: 2024 Status Update.

Bar-Even, A., Noor, E., Milo, R., 2012. A survey of carbon fixation pathways through a quantitative lens. J Exp Bot 63, 2325–2342. https://doi.org/10.1093/JXB/ERR417

Benz, G.T., 2011. Bioreactor Design for Chemical Engineers. Chem. Eng. Progress 21–26.

Bernal, V., Castaño-Cerezo, S., Cánovas, M., 2016. Acetate metabolism regulation in Escherichia coli: carbon overflow, pathogenicity, and beyond. Applied Microbiology and Biotechnology 2016 100:21 100, 8985–9001. https://doi.org/10.1007/S00253-016-7832-X

Bernal, V., Castaño-Cerezo, S., Gallego-Jara, J., Écija-Conesa, A., de Diego, T., Iborra, J.L., Cánovas, M., 2014. Regulation of bacterial physiology by lysine acetylation of proteins. N Biotechnol 31, 586–595. https://doi.org/10.1016/J.NBT.2014.03.002

Braide, D., Panaritis, C., Patience, G., Boffito, D.C., 2024. Gas to liquids (GTL) microrefinery technologies: A review and perspective on socio-economic implications. Fuel 375, 132385. https://doi.org/10.1016/J.FUEL.2024.132385

Brown, T.D.K., Jones-Mortimer, M.C., Kornberg, H.L., 1977. The enzymic interconversion of acetate and acetyl-coenzyme A in Escherichia coli. J Gen Microbiol 102, 327–336. https://doi.org/10.1099/00221287-102-2-327

Castaño-Cerezo, S., Bernal, V., Röhrig, T., Termeer, S., Cánovas, M., 2015. Regulation of acetate metabolism in Escherichia coli BL21 by protein Nε-lysine acetylation. Appl Microbiol Biotechnol 99, 3533–3545. https://doi.org/10.1007/S00253-014-6280-8

Castaño-Cerezo, S., Pastor, J.M., Renilla, S., Bernal, V., Iborra, J.L., Cánovas, M., 2009. An insight into the role of phosphotransacetylase (pta) and the acetate/acetyl-CoA node in Escherichia coli. Microb Cell Fact 8, 1–19. https://doi.org/10.1186/1475-2859-8-54

Castelvecchi, D., 2022. How the hydrogen revolution can help save the planet - and how it can't. Nature 611, 440–443. https://doi.org/10.1038/D41586-022-03699-0

Chen, J., Li, W., Zhang, Z.Z., Tan, T.W., Li, Z.J., 2018. Metabolic engineering of Escherichia coli for the synthesis of polyhydroxyalkanoates using acetate as a main carbon source. Microb Cell Fact 17, 1–12. https://doi.org/10.1186/S12934-018-0949-0

Chen, Y., Nielsen, J., 2016. Biobased organic acids production by metabolically engineered microorganisms. Curr Opin Biotechnol 37, 165–172. https://doi.org/10.1016/J.COPBIO.2015.11.004

Choi, Y.J., Lee, S.Y., 2013. Microbial production of short-chain alkanes. Nature 502, 571–574. https://doi.org/10.1038/NATURE12536

Chong, H., Yeow, J., Wang, I., Song, H., Jiang, R., 2013. Improving Acetate Tolerance of Escherichia coli by Rewiring Its Global Regulator cAMP Receptor Protein (CRP). PLoS One 8, e77422. https://doi.org/10.1371/JOURNAL.PONE.0077422

Cordell, W.T., Avolio, G., Takors, R., Pfleger, B.F., 2024. Genome reduction improves octanoic acid production in scale down bioreactors. Microb Biotechnol 17, e70034. https://doi.org/10.1111/1751-7915.70034

Cordell, W.T., Avolio, G., Takors, R., Pfleger, B.F., 2023. Milligrams to kilograms: making microbes work at scale. Trends Biotechnol 41, 1442–1457. https://doi.org/10.1016/J.TIBTECH.2023.05.002

Cortés-Peña, Y., 2020. Thermosteam: BioSTEAM's Premier Thermodynamic Engine. J Open Source Softw 5, 2814. https://doi.org/10.21105/JOSS.02814

Cortes-Peña, Y., Kumar, D., Singh, V., Guest, J.S., 2020. BioSTEAM: A Fast and Flexible Platform for the Design, Simulation, and Techno-Economic Analysis of Biorefineries under Uncertainty. ACS Sustain Chem Eng 8, 3302–3310. https://doi.org/10.1021/ACSSUSCHEMENG.9B07040

Cortés-Peña, Y.R., Kurambhatti, C., Eilts, K., Singh, V., Guest, J.S., 2022. Economic and Environmental Sustainability of Vegetative Oil Extraction Strategies at Integrated Oilcane and Oil-Sorghum Biorefineries. ACS Sustain Chem Eng 10, 13972–13979. https://doi.org/10.1021/ACSSUSCHEMENG.2C04204

Cortés-Peña, Y.R., Woodruff, W., Banerjee, S., Li, Y., Singh, V., Rao, C. V, Guest, J.S., 2024. Integration of Plant and Microbial Oil Processing at Oilcane Biorefineries for More Sustainable Biofuel Production. ChemRxiv. https://doi.org/10.26434/CHEMRXIV-2023-RDVBL-V2

Daza, Y.A., Kuhn, J.N., 2016. CO2 conversion by reverse water gas shift catalysis: comparison of catalysts, mechanisms and their consequences for CO2 conversion to liquid fuels. RSC Adv 6, 49675–49691. https://doi.org/10.1039/C6RA05414E

Dewes, I., Schumpe, A., 1997. Gas density effect on mass transfer in the slurry bubble column. Chem Eng Sci 52, 4105–4109. https://doi.org/10.1016/S0009-2509(97)00252-2

Enjalbert, B., Millard, P., Dinclaux, M., Portais, J.C., Létisse, F., 2017. Acetate fluxes in Escherichia coli are determined by the thermodynamic control of the Pta-AckA pathway. Scientific Reports 2017 7:1 7, 1–11. https://doi.org/10.1038/srep42135

Galán-Martín, Á., Tulus, V., Díaz, I., Pozo, C., Pérez-Ramírez, J., Guillén-Gosálbez, G., 2021. Sustainability footprints of a renewable carbon transition for the petrochemical sector within planetary boundaries. One Earth 4, 565–583. https://doi.org/10.1016/J.ONEEAR.2021.04.001

Gasparrini, W., Lee, S.H., Woolston, B.M., 2025. Pathways to sustainability: a quantitative comparison of aerobic and anaerobic C1 bioconversion routes. Curr Opin Biotechnol 93, 103310. https://doi.org/10.1016/J.COPBIO.2025.103310

Gifuni, I., Pollio, A., Safi, C., Marzocchella, A., Olivieri, G., 2019. Current Bottlenecks and Challenges of the Microalgal Biorefinery. Trends Biotechnol 37, 242–252. https://doi.org/10.1016/J.TIBTECH.2018.09.006

Hermann, T., 2003. Industrial production of amino acids by coryneform bacteria. J Biotechnol 104, 155–172. https://doi.org/10.1016/S0168-1656(03)00149-4

Hernández Lozada, N.J., Simmons, T.R., Xu, K., Jindra, M.A., Pfleger, B.F., 2020. Production of 1-octanol in Escherichia coli by a high flux thioesterase route. Metab Eng 61, 352–359. https://doi.org/10.1016/J.YMBEN.2020.07.004

Herwig, C., Martin Pereira De Pereira, C., Robert Bengelsdorf, F., Marcellin, E., Souza Pinto Lemgruber, de R., Heffernan, J.K., Valgepea, K., de Souza Pinto Lemgruber, R., Casini, I., Plan, M., Tappel, R., Simpson, S.D., Köpke, M., Nielsen, L.K., 2020. Enhancing CO2-Valorization Using Clostridium autoethanogenum for Sustainable Fuel and Chemicals Production. Front Bioeng Biotechnol 8, 485713. https://doi.org/10.3389/FBIOE.2020.00204

Hu, P., Chakraborty, S., Kumar, A., Woolston, B., Liu, H., Emerson, D., Stephanopoulos, G., 2016. Integrated bioprocess for conversion of gaseous substrates to liquids. Proc Natl Acad Sci U S A 113, 3773–3778. https://doi.org/10.1073/PNAS.1516867113

Huang, B., Yang, H., Fang, G., Zhang, X., Wu, H., Li, Z., Ye, Q., 2018. Central pathway engineering for enhanced succinate biosynthesis from acetate in Escherichia coli. Biotechnol Bioeng 115, 943–954. https://doi.org/10.1002/BIT.26528

Humbird, D., Davis, R., McMillan, J.D., 2017. Aeration costs in stirred-tank and bubble column bioreactors. Biochem Eng J 127, 161–166. https://doi.org/10.1016/J.BEJ.2017.08.006

Humbird, D., Davis, R., Tao, L., Kinchin, C., Hsu, D., Aden, A., Schoen, P., Lukas, J., Olthof, B., Worley, M., Sexton, D., Dudgeon, D., 2011. Process Design and Economics for Biochemical Conversion of Lignocellulosic Biomass to Ethanol: Dilute-Acid Pretreatment and Enzymatic Hydrolysis of Corn Stover. Golden, CO, Seattle, WA, Atlanta, GA.

Iram, A., Cekmecelioglu, D., Demirci, A., 2022. Integrating 1G with 2G Bioethanol Production by Using Distillers' Dried Grains with Solubles (DDGS) as the Feedstock for Lignocellulolytic Enzyme Production. Fermentation 2022, Vol. 8, Page 705 8, 705. https://doi.org/10.3390/FERMENTATION8120705

Jindra, M.A., Choe, K., Chowdhury, R., Kong, R., Ghaffari, S., Sweedler, J. V., Pfleger, B.F., 2023. Evaluation of strategies to narrow the product chain-length distribution of microbially synthesized free fatty acids. Metab Eng 77, 21–31. https://doi.org/10.1016/J.YMBEN.2023.02.012

Jo, M., Noh, M.H., Lim, H.G., Kang, C.W., Im, D.K., Oh, M.K., Jung, G.Y., 2019. Precise tuning of the glyoxylate cycle in Escherichia coli for efficient tyrosine production from acetate. Microb Cell Fact 18, 1–9. https://doi.org/10.1186/S12934-019-1106-0

Kiefer, D., Merkel, M., Lilge, L., Henkel, M., Hausmann, R., 2021. From Acetate to Bio-Based Products: Underexploited Potential for Industrial Biotechnology. Trends Biotechnol 39, 397–411. https://doi.org/10.1016/J.TIBTECH.2020.09.004

Kornberg, H.L., 1966. The role and control of the glyoxylate cycle in Escherichia coli. Biochemical Journal 99, 1. https://doi.org/10.1042/BJ0990001

Kumari, S., Tishel, R., Eisenbach, M., Wolfe, A.J., 1995. Cloning, characterization, and functional expression of acs, the gene which encodes acetyl coenzyme A synthetase in Escherichia coli. J Bacteriol 177, 2878–2886. https://doi.org/10.1128/JB.177.10.2878-2886.1995

Kurian, J. V., 2005. A new polymer platform for the future - Sorona® from corn derived 1,3-propanediol. J Polym Environ 13, 159–167. https://doi.org/10.1007/S10924-005-2947-7

Kutscha, R., Pflügl, S., 2020. Microbial Upgrading of Acetate into Value-Added Products—Examining Microbial Diversity, Bioenergetic Constraints and Metabolic Engineering Approaches. International Journal of Molecular Sciences 2020, Vol. 21, Page 8777 21, 8777. https://doi.org/10.3390/IJMS21228777

Kutscha, R., Tomin, T., Birner-Gruenberger, R., Bekiaris, P.S., Klamt, S., Pflügl, S., 2024. Efficiency of acetate-based isopropanol synthesis in Escherichia coli W is controlled by ATP demand. Biotechnology for Biofuels and Bioproducts 17, 1–19. https://doi.org/10.1186/S13068-024-02534-0

Lai, N., Luo, Y., Fei, P., Hu, P., Wu, H., 2021. One stone two birds: Biosynthesis of 3-hydroxypropionic acid from CO2 and syngas-derived acetic acid in Escherichia coli. Synth Syst Biotechnol 6, 144–152. https://doi.org/10.1016/J.SYNBIO.2021.06.003

Laura, M., Jo, P., 2023. No acetogen is equal: Strongly different H2 thresholds reflect diverse bioenergetics in acetogenic bacteria. Environ Microbiol 25, 2032–2040. https://doi.org/10.1111/1462-2920.16429

Lehtinen, T., Virtanen, H., Santala, S., Santala, V., 2018. Production of alkanes from CO2 by engineered bacteria. Biotechnol Biofuels 11, 1–11. https://doi.org/10.1186/S13068-018-1229-2

Lennen, R.M., Braden, D.J., West, R.M., Dumesic, J.A., Pfleger, B.F., 2010. A process for microbial hydrocarbon synthesis: Overproduction of fatty acids in Escherichia coli and catalytic conversion to alkanes. Biotechnol Bioeng 106, 193–202. https://doi.org/10.1002/BIT.22660

Lennen, R.M., Kruziki, M.A., Kumar, K., Zinkel, R.A., Burnum, K.E., Lipton, M.S., Hoover, S.W., Ranatunga, D.R., Wittkopp, T.M., Marner, W.D., Pfleger, B.F., 2011. Membrane stresses induced by overproduction of free fatty acids in Escherichia coli. Appl Environ Microbiol 77, 8114–8128. https://doi.org/10.1128/AEM.05421-11

Lennen, R.M., Pfleger, B.F., 2013. Microbial production of fatty acid-derived fuels and chemicals. Curr Opin Biotechnol 24, 1044–1053. https://doi.org/10.1016/J.COPBIO.2013.02.028

Lennen, R.M., Pfleger, B.F., 2012. Engineering Escherichia coli to synthesize free fatty acids. Trends Biotechnol 30, 659–667. https://doi.org/10.1016/J.TIBTECH.2012.09.006

Li, S., Ye, Z., Moreb, E.A., Hennigan, J.N., Castellanos, D.B., Yang, T., Lynch, M.D., 2021. Dynamic control over feedback regulatory mechanisms improves NADPH flux and xylitol biosynthesis in engineered E. coli. Metab Eng 64, 26–40. https://doi.org/10.1016/J.YMBEN.2021.01.005

Li, S.H.J., Li, Z., Park, J.O., King, C.G., Rabinowitz, J.D., Wingreen, N.S., Gitai, Z., 2018. Escherichia coli translation strategies differ across carbon, nitrogen and phosphorus limitation conditions. Nat Microbiol 3, 939–947. https://doi.org/10.1038/S41564-018-0199-2

Li, W., Chen, J., Liu, C.X., Yuan, Q.P., Li, Z.J., 2019. Microbial production of glycolate from acetate by metabolically engineered Escherichia coli. J Biotechnol 291, 41–45. https://doi.org/10.1016/J.JBIOTEC.2018.12.012

Li, Y., Kontos, G.A., Cabrera, D. V., Avila, N.M., Parkinson, T.W., Viswanathan, M.B., Singh, V., Altpeter, F., Labatut, R.A., Guest, J.S., 2023a. Design of a High-Rate Wastewater Treatment Process for Energy and Water Recovery at Biorefineries. ACS Sustain Chem Eng 11, 3861–3872. https://doi.org/10.1021/ACSSUSCHEMENG.2C07139

Li, Y., Kontos, G.A., Cabrera, D. V., Avila, N.M., Parkinson, T.W., Viswanathan, M.B., Singh, V., Altpeter, F., Labatut, R.A., Guest, J.S., 2023b. Design of a High-Rate Wastewater Treatment Process for Energy and Water Recovery at Biorefineries. ACS Sustain Chem Eng 11, 3861–3872. https://doi.org/10.1021/ACSSUSCHEMENG.2C07139

Li, Y., Trimmer, J.T., Hand, S., Zhang, X., Chambers, K.G., Lohman, H.A.C., Shi, R., Byrne, D.M., Cook, S.M., Guest, J.S., 2022. Quantitative sustainable design (QSD) for the prioritization of research, development, and deployment of technologies: a tutorial and review. Environ Sci (Camb) 8, 2439–2465. https://doi.org/10.1039/D2EW00431C

Liew, F.E., Nogle, R., Abdalla, T., Rasor, B.J., Canter, C., Jensen, R.O., Wang, L., Strutz, J., Chirania, P., De Tissera, S., Mueller, A.P., Ruan, Z., Gao, A., Tran, L., Engle, N.L., Bromley, J.C., Daniell, J., Conrado, R., Tschaplinski, T.J., Giannone, R.J., Hettich, R.L., Karim, A.S., Simpson, S.D., Brown, S.D., Leang, C., Jewett, M.C., Köpke, M., 2025. Addendum: Carbon-negative production of acetone and isopropanol by gas fermentation at

industrial pilot scale. Nature Biotechnology 2025 43:8 43, 1385–1387. https://doi.org/10.1038/s41587-025-02767-w

Liew, F.E., Nogle, R., Abdalla, T., Rasor, B.J., Canter, C., Jensen, R.O., Wang, L., Strutz, J., Chirania, P., De Tissera, S., Mueller, A.P., Ruan, Z., Gao, A., Tran, L., Engle, N.L., Bromley, J.C., Daniell, J., Conrado, R., Tschaplinski, T.J., Giannone, R.J., Hettich, R.L., Karim, A.S., Simpson, S.D., Brown, S.D., Leang, C., Jewett, M.C., Köpke, M., 2022. Carbon-negative production of acetone and isopropanol by gas fermentation at industrial pilot scale. Nat Biotechnol 40, 335–344. https://doi.org/10.1038/S41587-021-01195-W

Liew, F.M., Martin, M.E., Tappel, R.C., Heijstra, B.D., Mihalcea, C., Köpke, M., 2016. Gas Fermentation-A flexible platform for commercial scale production of low-carbon-fuels and chemicals from waste and renewable feedstocks. Front Microbiol 7, 202812. https://doi.org/10.3389/FMICB.2016.00694/XML

Long, B., Zhang, F., Dai, S.Y., Foston, M., Tang, Y.J., Yuan, J.S., 2025. Engineering strategies to optimize lignocellulosic biorefineries. Nature Reviews Bioengineering 3, 230–244. https://doi.org/10.1038/S44222-024-00247-5

Louw, J., Dogbe, E.S., Yang, B., Görgens, J.F., 2023. Prioritisation of biomass-derived products for biorefineries based on economic feasibility: A review on the comparability of techno-economic assessment results. Renewable and Sustainable Energy Reviews 188, 113840. https://doi.org/10.1016/J.RSER.2023.113840

Mains, K., Peoples, J., Fox, J.M., 2022. Kinetically guided, ratiometric tuning of fatty acid biosynthesis. Metab Eng 69, 209–220. https://doi.org/10.1016/J.YMBEN.2021.11.008

Maitah, M., Smutka, L., 2019. The Development of World Sugar Prices. Sugar Tech 21, 1–8. https://doi.org/10.1007/S12355-018-0618-Y

Materials Library | CatCost [WWW Document], n.d. URL https://catcost.chemcatbio.org/materials-library (accessed 7.10.25).

Mehrer, C.R., Incha, M.R., Politz, M.C., Pfleger, B.F., 2018. Anaerobic production of medium-chain fatty alcohols via a β-reduction pathway. Metab Eng 48, 63–71. https://doi.org/10.1016/J.YMBEN.2018.05.011

Miao, R., Xie, H., Liu, X., Lindberg, P., Lindblad, P., 2020. Current processes and future challenges of photoautotrophic production of acetyl-CoA-derived solar fuels and chemicals in cyanobacteria. Curr Opin Chem Biol 59, 69–76. https://doi.org/10.1016/J.CBPA.2020.04.013

Nakamura, C.E., Whited, G.M., 2003. Metabolic engineering for the microbial production of 1,3-propanediol. Curr Opin Biotechnol 14, 454–459. https://doi.org/10.1016/J.COPBIO.2003.08.005

Neidhardt, F.C., Bloch, P.L., Smith, D.F., 1974. Culture Medium for Enterobacteria. J Bacteriol 119, 736–747. https://doi.org/10.1128/JB.119.3.736-747.1974

Noh, M.H., Lim, H.G., Woo, S.H., Song, J., Jung, G.Y., 2018. Production of itaconic acid from acetate by engineering acid-tolerant Escherichia coli W. Biotechnol Bioeng 115, 729–738. https://doi.org/10.1002/BIT.26508

Novak, K., Flöckner, L., Erian, A.M., Freitag, P., Herwig, C., Pflügl, S., 2018. Characterizing the effect of expression of an acetyl-CoA synthetase insensitive to acetylation on co-utilization of glucose and acetate in batch and continuous cultures of E. coli W. Microb Cell Fact 17, 1–15. https://doi.org/10.1186/S12934-018-0955-2

Novak, K., Kutscha, R., Pflügl, S., 2020. Microbial upgrading of acetate into 2,3-butanediol and acetoin by E. coli W. Biotechnol Biofuels 13, 1–14. https://doi.org/10.1186/S13068-020-01816-7

Park, K., Quach, T., Clark, T.J., Kim, H., Zhang, T., Wang, M., Guo, M., Sato, S., Nazarenus, T.J., Blume, R., Blume, Y., Zhang, C., Moose, S.P., Swaminathan, K., Schwender, J., Clemente, T.E., Cahoon, E.B., 2025. Development of vegetative oil sorghum: From lab-to-field. Plant Biotechnol J 23, 660–673. https://doi.org/10.1111/PBI.14527

Perry, R.H., Green, D.W., Maloney, J.O. (Eds.), 1997. Perry's Chemical Engineer's Handbook, 7th ed. McCraw-Hill, New York.

Pfleger, B.F., 2016. Microbes paired for biological gas-to-liquids (Bio-GTL) process. Proc Natl Acad Sci U S A 113, 3717–3719. https://doi.org/10.1073/PNAS.1601926113

Pfleger, B.F., Takors, R., 2023. Recent progress in the synthesis of advanced biofuel and bioproducts. Curr Opin Biotechnol 80, 102913. https://doi.org/10.1016/J.COPBIO.2023.102913

Pinheiro, L.P., Longati, A.A., Elias, A.M., Perez, C.L., Pereira, L.P.R. da C., Zangirolami, T.C., Furlan, F.F., Giordano, R. de C., Milessi, T.S., 2025. Improving the Feasibility of 2G Ethanol Production from Lignocellulosic Hydrolysate Using Immobilized Recombinant Yeast: A Technical–Economic Analysis and Life Cycle Assessment. Fermentation 11, 116. https://doi.org/10.3390/FERMENTATION11030116

Poehlein, A., Zeldes, B., Flaiz, M., Böer, T., Lüschen, A., Höfele, F., Baur, K.S., Molitor, B., Kröly, C., Wang, M., Zhang, Q., Fan, Y., Chao, W., Daniel, R., Li, F., Basen, M., Müller, V., Angenent, L.T., Sousa, D.Z., Bengelsdorf, F.R., 2025. Advanced aspects of acetogens. Bioresour Technol 427, 131913. https://doi.org/10.1016/J.BIORTECH.2024.131913

Rabbers, I., Gottstein, W., Feist, A.M., Teusink, B., Bruggeman, F.J., Bachmann, H., 2022. Selection for Cell Yield Does Not Reduce Overflow Metabolism in Escherichia coli. Mol Biol Evol 39. https://doi.org/10.1093/MOLBEV/MSAB345

Rahman, A., Murad, S.M.W., Mohsin, A.K.M., Wang, X., 2024. Does renewable energy proactively contribute to mitigating carbon emissions in major fossil fuels consuming countries? J Clean Prod 452, 142113. https://doi.org/10.1016/J.JCLEPRO.2024.142113

Ricci, L., Cen, X., Zu, Y., Antonicelli, G., Chen, Z., Fino, D., Pirri, F.C., Stephanopoulos, G., Woolston, B.M., Re, A., 2025. Metabolic Engineering of E. coli for Enhanced Diols Production from Acetate. ACS Synth Biol 14, 1204–1219. https://doi.org/10.1021/ACSSYNBIO.4C00839

Schastnaya, E., Doubleday, P.F., Maurer, L., Sauer, U., 2023. Non-enzymatic acetylation inhibits glycolytic enzymes in Escherichia coli. Cell Rep 42, 111950. https://doi.org/10.1016/J.CELREP.2022.111950

Schowanek, D., Borsboom-Patel, T., Bouvy, A., Colling, J., de Ferrer, J.A., Eggers, D., Groenke, K., Gruenenwald, T., Martinsson, J., Mckeown, P., Miller, B., Moons, S., Niedermann, K., Pérez, M., Schneider, C., Viot, J.F., 2018. New and updated life cycle inventories for surfactants used in European detergents: summary of the ERASM surfactant life cycle and ecofootprinting project. International Journal of Life Cycle Assessment 23, 867–886. https://doi.org/10.1007/S11367-017-1384-X

Schuchmann, K., Müller, V., 2014. Autotrophy at the thermodynamic limit of life: A model for energy conservation in acetogenic bacteria. Nat Rev Microbiol 12, 809–821. https://doi.org/10.1038/NRMICRO3365

Seider, W.D., Lewin, D.R., Seader, J.D., Widagdo, S., Gani, R., Ng, K.M., 2016. Product and process design principles: synthesis, analysis and evaluation, Product and process desing principles. John Wiley & Sons.

Shah, J., Arslan, E., Cirucci, J., O'Brien, J., Moss, D., 2016. Comparison of Oleo- vs Petro-Sourcing of Fatty Alcohols via Cradle-to-Gate Life Cycle Assessment. J Surfactants Deterg 19, 1333–1351. https://doi.org/10.1007/S11743-016-1867-Y

Shiba, Y., Paradise, E.M., Kirby, J., Ro, D.K., Keasling, J.D., 2007. Engineering of the pyruvate dehydrogenase bypass in Saccharomyces cerevisiae for high-level production of isoprenoids. Metab Eng 9, 160–168. https://doi.org/10.1016/J.YMBEN.2006.10.005

Shiloach, J., Fass, R., 2005. Growing E. coli to high cell density—A historical perspective on method development. Biotechnol Adv 23, 345–357. https://doi.org/10.1016/J.BIOTECHADV.2005.04.004

Shimizu, K., 2013. Regulation Systems of Bacteria such as Escherichia coli in Response to Nutrient Limitation and Environmental Stresses. Metabolites 2014, Vol. 4, Pages 1-35 4, 1–35. https://doi.org/10.3390/METABO4010001

Shin, K.S., Kim, S., Lee, S.K., 2016. Improvement of free fatty acid production using a mutant acyl-CoA thioesterase I with high specific activity in Escherichia coli. Biotechnol Biofuels 9, 1–10. https://doi.org/10.1186/S13068-016-0622-Y

Soma, Y., Tsuruno, K., Wada, M., Yokota, A., Hanai, T., 2014. Metabolic flux redirection from a central metabolic pathway toward a synthetic pathway using a metabolic toggle switch. Metab Eng 23, 175–184. https://doi.org/10.1016/j.ymben.2014.02.008

Song, H.S., Seo, H.M., Jeon, J.M., Moon, Y.M., Hong, J.W., Hong, Y.G., Bhatia, S.K., Ahn, J., Lee, H., Kim, W., Park, Y.C., Choi, K.Y., Kim, Y.G., Yang, Y.H., 2018. Enhanced isobutanol production from acetate by combinatorial overexpression of acetyl-CoA synthetase and anaplerotic enzymes in engineered Escherichia coli. Biotechnol Bioeng 115, 1971–1978. https://doi.org/10.1002/BIT.26710

Song, Y., Prather, K.L.J., 2024. Strategies in engineering sustainable biochemical synthesis through microbial systems. Curr Opin Chem Biol 81, 102493. https://doi.org/10.1016/J.CBPA.2024.102493

Starai, V.J., Escalante-Semerena, J.C., 2004. Identification of the Protein Acetyltransferase (Pat) Enzyme that Acetylates Acetyl-CoA Synthetase in Salmonella enterica. J Mol Biol 340, 1005–1012. https://doi.org/10.1016/J.JMB.2004.05.010

Starai, V.J., Gardner, J.G., Escalante-Semerena, J.C., 2005. Residue Leu-641 of Acetyl-CoA Synthetase is Critical for the Acetylation of Residue Lys-609 by the Protein Acetyltransferase Enzyme of Salmonella enterica. Journal of Biological Chemistry 280, 26200–26205. https://doi.org/10.1074/JBC.M504863200

Stark, C., Münßinger, S., Rosenau, F., Eikmanns, B.J., Schwentner, A., 2022. The Potential of Sequential Fermentations in Converting C1 Substrates to Higher-Value Products. Front Microbiol 13, 907577. https://doi.org/10.3389/FMICB.2022.907577

Stocker, T.F., Qin, D., Plattner, G.-K., Tignor, M., Allen, S.K., Boschung, J., Nauels, A., Xia, Y., Bex, V., Midgley, P.M., 2013. IPCC, 2013: Climate Change 2013: The Physical Science Basis. Contribution of Working Group I to the Fifth Assessment Report of the Intergovernmental Panel on Climate Change. Cambridge University Press, Cambridge, United Kingdom and New York, NY, USA.

Su, Y., Mangus, A.M., Cordell, W.T., Pfleger, B.F., 2024. Overcoming barriers to medium-chain fatty alcohol production. Curr Opin Biotechnol 85, 103063. https://doi.org/10.1016/J.COPBIO.2023.103063

Sugar - Price - Chart - Historical Data - News [WWW Document], n.d. URL https://tradingeconomics.com/commodity/sugar (accessed 7.10.25).

Sulis, D.B., Lavoine, N., Sederoff, H., Jiang, X., Marques, B.M., Lan, K., Cofre-Vega, C., Barrangou, R., Wang, J.P., 2025. Advances in lignocellulosic feedstocks for bioenergy and

bioproducts. Nature Communications 2025 16:1 16, 1–13. https://doi.org/10.1038/s41467-025-56472-y

Sun, X., Shen, X., Jain, R., Lin, Y., Wang, Jian, Sun, J., Wang, Jia, Yan, Y., Yuan, Q., 2015. Synthesis of chemicals by metabolic engineering of microbes. Chem Soc Rev 44, 3760–3785. https://doi.org/10.1039/C5CS00159E

Sun, Y.Q., Shen, J.T., Yan, L., Zhou, J.J., Jiang, L.L., Chen, Y., Yuan, J.L., Feng, E.M., Xiu, Z.L., 2018. Advances in bioconversion of glycerol to 1,3-propanediol: Prospects and challenges. Process Biochemistry 71, 134–146. https://doi.org/10.1016/J.PROCBIO.2018.05.009

Thompson, J., Tyner, W.E., 2011. Corn stover for Bioenergy Production: Cost estimates and Farmer supply response Fueling and Feeding America Through Renewable Resources.

Valgepea, K., Adamberg, K., Nahku, R., Lahtvee, P.J., Arike, L., Vilu, R., 2010. Systems biology approach reveals that overflow metabolism of acetate in Escherichia coli is triggered by carbon catabolite repression of acetyl-CoA synthetase. BMC Syst Biol 4, 1–13. https://doi.org/10.1186/1752-0509-4-166

Van'T Riet, K., 1979. Review of Measuring Methods and Results in Nonviscous Gas-Liquid Mass Transfer in Stirred Vessels. Industrial and Engineering Chemistry Process Design and Development 18, 357–364. https://doi.org/10.1021/I260071A001

Vickers, J., Peterson, D., Randolph, K., 2020. DOE Hydrogen and Fuel Cells Program Record (#20004): Cost of Electrolytic Hydrogen Production with Existing Technology. U.S. Deparment of Energy.

Wang, M., Elgowainy, A., Lee, U., Baek, K.H., Balchandani, S., Benavides, P.T., Burnham, A., Cai, H., Chen, P., Gan, Y., Gracida-Alvarez, U.R., Hawkins, T.R., Huang, T.-Y., Iyer, K.R., Kar, S., Kelly, J.C., Kim, T., Kolodziej, C.P., Lee, K., Liu, X., Lu, Z., Masum, F.H., Morales, M., Ng, C., Ou, L., Poddar, T.K., Reddi, K., Shukla, S., Singh, U., Sun, L., Sun, P., Sykora, T., Vyawahare, P., Zhang, J., 2023. Summary of Expansions and Updates in R&D GREET ® 2023.

Watson, M.J., Machado, P.G., da Silva, A. V., Saltar, Y., Ribeiro, C.O., Nascimento, C.A.O., Dowling, A.W., 2024. Sustainable aviation fuel technologies, costs, emissions, policies, and markets: A critical review. J Clean Prod 449, 141472. https://doi.org/10.1016/J.JCLEPRO.2024.141472

Wichmann, J., Lauersen, K.J., Biondi, N., Christensen, M., Guerra, T., Hellgardt, K., Kühner, S., Kuronen, M., Lindberg, P., Rösch, C., Yunus, I.S., Jones, P., Lindblad, P., Kruse, O., 2021. Engineering Biocatalytic Solar Fuel Production: The PHOTOFUEL Consortium. Trends Biotechnol 39, 323–327. https://doi.org/10.1016/J.TIBTECH.2021.01.003

Wood, D.A., Nwaoha, C., Towler, B.F., 2012. Gas-to-liquids (GTL): A review of an industry offering several routes for monetizing natural gas. J Nat Gas Sci Eng 9, 196–208. https://doi.org/10.1016/J.JNGSE.2012.07.001

Wu, J., Zhou, L., Duan, X., Peng, H., Liu, S., Zhuang, Q., Pablo, C.M., Fan, X., Ding, S., Dong, M., Zhou, J., 2021. Applied evolution: Dual dynamic regulations-based approaches in engineering intracellular malonyl-CoA availability. Metab Eng 67, 403–416. https://doi.org/10.1016/J.YMBEN.2021.08.004

Wu, W., Long, M.R., Zhang, X., Reed, J.L., Maravelias, C.T., 2018. A framework for the identification of promising bio-based chemicals. Biotechnol Bioeng 115, 2328–2340. https://doi.org/10.1002/BIT.26779

Xiao, Y., Ruan, Z., Liu, Z., Wu, S.G., Varman, A.M., Liu, Y., Tang, Y.J., 2013. Engineering Escherichia coli to convert acetic acid to free fatty acids. Biochem Eng J 76, 60–69. https://doi.org/10.1016/J.BEJ.2013.04.013

Xu, X., Xian, M., Liu, H., 2017. Efficient conversion of acetate into phloroglucinol by recombinant Escherichia coli. RSC Adv 7, 50942–50948. https://doi.org/10.1039/C7RA09519H

Xu, X., Xie, M., Zhao, Q., Xian, M., Liu, H., 2018. Microbial production of mevalonate by recombinant Escherichia coli using acetic acid as a carbon source. Bioengineered 9, 116–123. https://doi.org/10.1080/21655979.2017.1323592

Yang, H., Huang, B., Lai, N., Gu, Y., Li, Z., Ye, Q., Wu, H., 2019. Metabolic engineering of Escherichia coli carrying the hybrid acetone-biosynthesis pathway for efficient acetone biosynthesis from acetate Long Liu. Microb Cell Fact 18, 1–9. https://doi.org/10.1186/S12934-019-1054-8

Yang, H., Zhang, C., Lai, N., Huang, B., Fei, P., Ding, D., Hu, P., Gu, Y., Wu, H., 2020. Efficient isopropanol biosynthesis by engineered Escherichia coli using biologically produced acetate from syngas fermentation. Bioresour Technol 296, 122337. https://doi.org/10.1016/J.BIORTECH.2019.122337

Ye, Z., Li, S., Hennigan, J.N., Lebeau, J., Moreb, E.A., Wolf, J., Lynch, M.D., 2021. Two-stage dynamic deregulation of metabolism improves process robustness & scalability in engineered E. coli. Metab Eng 68, 106–118. https://doi.org/10.1016/J.YMBEN.2021.09.009

Youngquist, J.T., Korosh, T.C., Pfleger, B.F., 2017. Functional Genomics Analysis of Free Fatty Acid Production under Continuous Phosphate Limiting Conditions. J Ind Microbiol Biotechnol 44, 759. https://doi.org/10.1007/S10295-016-1846-3

Youngquist, J.T., Rose, J.P., Pfleger, B.F., 2013a. Free fatty acid production in Escherichia coli under phosphate-limited conditions. Appl Microbiol Biotechnol 97, 5149–5159. https://doi.org/10.1007/S00253-013-4911-0

Youngquist, J.T., Schumacher, M.H., Rose, J.P., Raines, T.C., Politz, M.C., Copeland, M.F., Pfleger, B.F., 2013b. Production of medium chain length fatty alcohols from glucose in Escherichia coli. Metab Eng 20, 177–186. https://doi.org/10.1016/J.YMBEN.2013.10.006

Zha, W., Rubin-Pitel, S.B., Shao, Z., Zhao, H., 2009. Improving cellular malonyl-CoA level in Escherichia coli via metabolic engineering. Metab Eng 11, 192–198. https://doi.org/10.1016/J.YMBEN.2009.01.005

Zhang, C., Fei, Q., Fu, R., Lackner, M., Zhou, Y.J., Tan, T., 2025. Economic and sustainable revolution to facilitate one-carbon biomanufacturing. Nature Communications 2025 16:1 16, 1–10. https://doi.org/10.1038/s41467-025-60247-w

Zhang, W., Zhang, H., Shang, Y., Luo, Y., Wu, Haizhen, Wu, Hui, 2025. High-Yield Biosynthesis of 3-Hydroxypropionic Acid from Acetate in Metabolically Engineered Escherichia coli. ACS Synth Biol 14, 1654–1666. https://doi.org/10.1021/ACSSYNBIO.5C00030

Zuiderveen, E.A.R., Kuipers, K.J.J., Caldeira, C., Hanssen, S. V., van der Hulst, M.K., de Jonge, M.M.J., Vlysidis, A., van Zelm, R., Sala, S., Huijbregts, M.A.J., 2023. The potential of emerging bio-based products to reduce environmental impacts. Nat Commun 14, 1–7. https://doi.org/10.1038/S41467-023-43797-9